GROUND MOTION SCALING IN THE MARMARA REGION, TURKEY

[(1)]Akinci, A., [(1)] Malagnini, L., [(2)] Herrmann, R.B., [(3)] Gok, R and [(4)] Sørensen, M. B.

(1) Istituto Nazionale di Geofisica e Vulcanologia, Via di Vigna Murata 605, 00143 Roma, Italy

(2) Department of Earth and Atmospheric Sciences, Saint Louis University, 3507 Laclede Ave. St. Louis, MO 63103 USA

(3) Lawrence Livermore National Laboratory, Earth Sciences Division L-206 7000 East Ave Livermore, California, USA

(4) Department of Earth Science, University of Bergen, Allegaten 41, 5007 Bergen, Norway

Geophysical Journal International

January 2006

Summary

Predictive relationships for the ground motion in the Marmara region (north-western Turkey) are parameterized after regressing three-component waveforms from regional earthquakes, in the frequency range: 0.4-15.0 Hz, and in the distance range: 10 - 200 km. The data set consists of 2400 three-component recordings from 462 earthquakes, recorded at 53 stations. Moment magnitudes, M_w, range between 2.5 and 7.2. The largest event for which we have waveforms available (M_w 7.2) occurred in Duzce on November 12, 1999. The aftershocks of that earthquake, together with the aftershocks of the August 17, 1999 Izmit event (M_w = 7.4), are included in the dataset.

Regressions are performed, independently, on Fourier velocity spectra and on peak ground velocities, for a large number of sampling frequencies. A simple model is used to relate the logarithm of the measured ground motion to excitation, site, and propagation terms. Results obtained for peak velocities are used to define a piecewise continuous geometrical spreading function, *g(r),* a frequency-dependent *Q(f),* and a distance-dependent duration function. The latter is used, through random vibration theory (RVT), in order to predict time-domain characteristics (i.e., peak values) of the ground motion. The complete model obtained for the peak ground motion was used to match the results of the regressions on the Fourier amplitudes.

Fourier velocity spectra for the combined horizontal motion are best fit by a hinged quadri-linear geometrical spreading function for observations in the 10 – 200 km hypocentral distances range as a function of frequency: ***f < 1.0 Hz,*** $r^{-1.2}$ for $r \leq 30$ km; $r^{-0.7}$ for $30 < r \leq 60$ km; $r^{-1.4}$ for $60 < r \leq 100$ km; $r^{-0.1}$ for $r > 100$,

f ≥ 1.0Hz, $r^{-1.0}$ for $r \leq 30$ km; $r^{-0.6}$ for $30 < r \leq 60$ km; $r^{-0.9}$ for $60 < r \leq 100$ km; $r^{-0.1}$ for r > 100 km. The frequency dependent crustal shear-wave quality factor Q (f) coefficient $Q(f) = 180\, f^{0.45}$. The *T (5-75%)* duration window provides good agreement between observed and predicted peak values. By modeling the behavior of the small earthquakes at high frequency, we also quantified a regional parameter κ=0.055 sec. Spectral models with one single-corner frequency (Brune), and with two corner frequencies (Atkinson and Silva, 2000) fit the observed high frequency excitation levels equally well, whereas the model by Atkinson and Silva (2000) fits the low frequency observations slightly better than the Brune's one.

Random Vibration Theory (RVT) is used to predict the absolute levels of ground shaking, following Boore's (1996) implementation of the stochastic ground motion model (Boore's SMSIM codes). Our regional empirical predictive relationships are compared to the ones adopted in several regions of the world, from California to Western United States (U.S.).

Keywords: Marmara Region, Turkey, Attenuation, Ground Motion Scaling.

Introduction

A significant proportion of Turkey is subjected to frequent and damaging earthquakes. Turkey is located on the relatively small Anatolian plate, which is being squeezed between three other major tectonic plates, the north-moving African and Arabian plates, which are both colliding with the Eurasian plate. As a consequence of the complex tectonics, the Anatolian plate is forced to move westward, into the Aegean Sea, through relatively simple fault systems located at the boundaries between plates. The most

important of these systems is the North Anatolian Fault Zone (NAFZ, Sengor et al., 1985).

The NAFZ is a relatively simple, narrow, right-lateral strike-slip fault zone. It is defined quite obviously by surface ruptures, along almost its entire length (over 1000 km). Most of the length of the NAFZ was broken by a series of large earthquakes between 1939 and 1967 (Fig.1). In the vicinity of the Sea of Marmara, the NAFZ splits into several fault strands, and the deformation becomes distributed over a broad zone, ~120 km wide. The two largest event (M_w=7.4 and M_w=7.2) occurred on the northern branch of the NAFZ on August 17 and November 12, 1999, respectively.

Along the northern shoreline of the Gulf of Izmit is a major industrial area, whereas the adjacent area to the south is predominantly residential and heavily populated. The damage caused by the 17 August 1999 earthquake was extensive. According to official data, this catastrophic event resulted in 17.127 casualties, 43.953 injuries and nearly 600.000 homeless. 77.342 buildings collapsed, including residential buildings and 77.169 buildings were moderately damaged, including residential buildings. Apart from the casualties, economic losses were substantial. Estimates of property loss, according to the World Bank report, Sept. 14, 1999, range from $3 billion to $6.5 billion, equivalent to 1.5 to 3.3 percent of the annual Gross National Product of Turkey.

Because of the real earthquake threat in the Marmara region, the need for seismic hazard studies has become progressively more important for earthquake engineering applications. A fundamental requirement for these studies is the determination of predictive relationships for the ground motion (Kramer, 1996). A number of such relationships have been developed for many regions of the world (Ambraseys et al.,

1996; Boore and Joyner, 1991; Boore, 1983; Toro and McGuire, 1987; Atkinson and Boore, 1995; Atkinson and Silva, 1987; Campell, 1997; Sadigh, 1997), mainly by regressing strong-motion data. These studies have shown that the ground motion levels can differ significantly in different tectonic regimes, for example depending on whether stresses are extensional or compressional.

However, in many parts of the world there are too few, or no, strong-motion recordings, and no strong-motion predictive relationships can be derived specifically for these regions. In these cases, it is necessary to adopt results obtained elsewhere, and use relationships from regions with comparable geology, tectonics, and seismicity. As an alternative, a number of papers have been published recently (e.g., Malagnini *et al*., 2002; Akinci *et al*., 2001; Bodin *et al*., 2004) on the determination of some aspects of ground motion scaling in various regions of the world by exploiting large amounts of data from the background seismicity. These studies have used weak- and strong-motion recordings for deriving predictive relationships.

Until recently the predictve relationships adopted for Turkey (mainly, for the Marmara region) were taken from the Western U.S. and California because of the similarities of the tectonic environments. In order to obtain regionalized attenuation relationships for the Marmara region, Ozbey *et al*. (2004) used the strong motion records from stations recently operated by Kandilli Observatory and Earthquake Research Institute (KOERI), Bogazici University , Istanbul Technical University (ITU), and Earthquake Research Department (ERD), General Directorate of Disaster Affairs. They used 195 strong motion records from 17 earthquakes, including the Izmit (M_w 7.4) and Duzce (M_w 7.2)

earthquakes and their aftershocks, as well as other events with magnitude M > 5.0. They compared their proposed model to predictions based on Western US empirical attenuation models for shallow crustal zones, and pointed out that the Western US models overpredict ground motions: in same cases, the Western US based predictions differed more than one standard deviation from those of the their Marmara model.

The objective of this study is to characterize ground motion observations in the Marmara region, using data from the network deployed after the 17 August 1999, Izmit earthquake. Predictive relationships are obtained through Random Vibration Theory (RVT) (Boore, 1983), which requires signal duration and amplitude spectra to estimate peak motions. Thus, we use seismograms from the large amount of aftershock data recorded by the micro-seismic networks instead of trying to reproduce the details of the high-frequency ground motion in the time domain, we use a source model and a regional scaling law to predict spectral shape and amplitude of ground motion at various source-receiver distances. At a set of sampling frequencies, we regress the peak values of narrow bandpass-filtered ground velocity time histories, as well as RMS-average Fourier spectral amplitudes, and define a regional predictive relationship characterized by a piece-wise linear geometric spreading (in a log-log space), a frequency-dependent crustal Q(f), and a function describing the effective duration of the ground motion in the region. The excitation spectral model contains the competing effects of an effective stress parameter, $\Delta\sigma$, of Brune's single-corner source model and a high-frequency attenuation term exp $(-\pi\kappa f)$. Using all the described information, then we obtain estimates of pseudo spectral acceleration (PSA), using the SMSIM (Stochastic Model SIMulation) codes of Boore (1996).

Seismological and Geological Background

The Marmara region is located at the western end of the NAFZ. The NAFZ extends for about 1500 km from Karliova, in the east, to the Aegean Sea at its western end. The NAFZ is a transitional structure: transpressional in its eastern part, it borders the Northern Anatolian Block, in a transtensional regime and reaches the extensional region of the Aegean Sea.

The NAFZ is an intercontinental dextral strike-slip fault, which comprises the boundary between Eurasia to the north and the Anatolian block to the south. Comparable in length and seismicity with the San Andreas Fault in California, it accommodates the westward extrusion of the Anatolian plate caused by the collision between the Arabian and the Eurasian plates in Eastern Anatolia (e.g. McKenzie 1972). The cumulative displacement along the fault is estimated to be about 40 km in the eastern section of the fault zone, and 20–30 km in its western end (e.g. Barka 1992). Recently, displacement rates of 22±3 mm yr^{-1} are obtained from GPS data (Straub and Kahle, 1997). East of longitude 32^0E, the deformation is related to the extrusion process, and the deformation is localized on a fault system that is several km wide. West of 32^0E, the fault splits into several branches, and deformation is rather distributed (e.g. Michel 1994). A major structural feature in the western part of the fault system is a tensional bend, displacing the main fault by about 25 km to the north (Fig. 1). At about 30.4^0 - 30.6^0 E, the bending trace of the main fault intersects two ENE-striking strands of the fault system. The junction area is seismically active and characterized by a mixture of earthquake mechanisms (Neugebauer *et al*. 1997).

The westernmost section of the NAFZ in the Sea of Marmara, is a large pull-apart basin, which appears to have been a geometrical/mechanical obstacle encountered by the NAFZ during its propagation. An outstandingly clear submarine morphology reveals a segmented fault system, including pull-apart features at a range of scales, indicating a dominant transtensional tectonic regime. Moreover, it has been observed that the NAF is continuous beneath the Sea of Marmara (Okay et al., 2000; Le Pichon et al., 2001), so it has no significant fault offsets that could stop a fault rupture.

This result is critical for understanding the seismic behavior of this region of the NAFZ, close to Istanbul. A series of strong earthquakes broke the NAFZ from east to west, starting with the destructive *M*s = 7.4, Erzincan earthquake of 1939, and ending with the 1999 Izmit and Duzce individual events. Even if we include the 1912 Galipoli earthquake, M_w=7.2, which occurred west of the Marmara Sea, there is still a gap corresponding to the branch of the NAF which crosses the northern border of the Marmara Sea (Ambraseys, 1970, 1975; Stein *et al*., 1997; Barka 1992). This gap has a length of 150 km and is therefore capable of generating an earthquake with magnitude similar to that of the Izmit earthquake (Hubert-Ferrari *et al.,* 2000; Parsons *et al.,* 2000).

The return period for large earthquakes south of Istanbul varies between 100-1000 years depending on the magnitude of earthquakes. The last major large earthquake on this segment was probably in 1509AD, (intensity, IX), (Barka, 1992, 1997-poly-project). The westward sequential progression of $M_w > 6.7$ earthquakes along the NAFZ during the 20^{th} century was studied by Stein *et al*., (1997) and by Nalbant *et al*., (1998). Stein *et al*. (1997) showed the earthquake-induced Coulomb stress changes on adjacent fault segments. Application of this technique to evaluate the effect of the Izmit earthquake on

neighboring faults, shows an area of increased stress to the east, including the Düzce fault which ruptured just after the Izmit earthquake (12 November, 1999, M_w=7.2). To the west, both the 80 km-long Yalova segment, southeast of Istanbul, and the Northern Boundary fault, immediately south of Istanbul, may be close to failure (Hubert-Ferrari *et al*., 2000).

Data

Following the destructive 1999 earthquakes, permanent regional earthquake monitoring was augmented through the temporary deployed instruments by United States Geological Survey (USGS), Lamont Doherty Earth Observatory-USA (LDEO), the permanent and temporary deployments of Earthquake Research Directorate, Ministry of Public Works and Reconstruction -Turkey (ERD), as well as the permanent deployed broadband stations of Bogazici University, Kandilli Observatory and Earthquake Research Institute (KOERI), among others. In this study, we used data recorded by 53 three-component digital stations after the 17 August 1999, Izmit earthquake (M_w=7.4). The digital waveform data from these deployments was assembled and made available in the CDROM distributed by the USGS and at web page http://geopubs.wr.usgs.gov/open-file/of01-163/ (Celebi et al., 2001). The data sampling frequency of strong motion records are 100 SPS (USGS Golden and Menlo Park, LDEO, ERD) as well as the broadband stations of KOERI. Magnitude and location calculation plays an important role in KOERI's activities and currently they report duration magnitude (M_d), local magnitude (M_L), and moment magnitude (M_w). The details about the data set and network is given by Celebei *et al*., (2001) in detail and is briefly discussed here. Gok and

Hutchings (2006) have uniformed the data correcting with instrumental responses and converting the whole dataset into a single unit (cm/sec^2).

The locations of the seismic stations and of selected events used at epicentral distances between 5 and 250 km are shown in Fig. 2. The 462 events in the data set span a magnitude range from 2.5 to 7.2 (Fig. 3). We only used unclipped and high signal/noise ratio data recorded in the time window 17 August 1999 - 30 November 2000. Fig. 4 displays the spatial distribution of the recordings at each station, as a function of hypocentral distance. We note that the spatial sampling of the available recordings is extremely dense and well distributed, at least out to a 200-km hypocentral distances. This characteristic leads to excellent regression results. The large amount of the data used in this study, recorded by LDEO, ERD and Geological and Earthquake Hazard Team of USGS. The data quality is confirmed with the existing M_w obtained from waveform inversion by Orgulu *et al* (2001) and with the coda method estimations by Mayeda *et al* (2005). Locations and the source parameters of the 30 aftershocks of the August 17, 1999 Izmit earthquake, $4.0<M_w<5.9$ are given by Orgulu and Aktar (2001).

Due to the heterogeneity of the surface geology in the region, the stations were deployed on different kinds of geologic outcrops. They are mostly deployed on unconsolidated sediments or in a building where the man made noise level was high. More information related with the stations site can be found in the distributed CD. The S/N of the KOERI broadband stations is better than the others since they were buried in few meters below the surface.

Ground Motion Regression

Regression analysis for both peak motion and Fourier velocity spectra are performed using a simple model. Assuming that the observed spectra can be described as a convolution of source, regional propagation, and site transfer functions, the logarithm of the spectral amplitude of the ground motion observed on the *k*-th waveform (the RMS-average taken within a frequency band logarithmically centered at the sampling frequency), relative to the *i*-th source and recorded at the *j*-th site, can be written as follows:

$$AMP_{kij}(f) = \log amp_{kij}(f) = EXC_i(f) + D(r_{ij}, r_{ref}, f) + SITE_j(f) \qquad (1)$$

where EXC_i is an excitation term, referred to a suitable reference distance from the source, $SITE_j$ is a site term (relative to an average site, see below), and $D(r_{ij}, r_{ref}, f)$ is the crustal propagation term, expressing the combined effect of geometrical spreading g(r) and the anelastic attenuation, Q(f). The propagation term is normalized to a null value at a reference hypocentral distance r_{ref} (see below).

With the implicit use of RVT, and of the Parseval's theorem, one can also write the logarithm of the peak amplitude of a relatively narrow bandpass-filtered time history around the frequency f, as the sum of source, propagation, and site terms:

$$PEAK_{kij}(f) = \log peak_{kij} = EXC_i(f) + D(r_{ij}, r_{ref}, f) + SITE_j(f) \qquad (2)$$

Although equations (1 and 2) are simple in appearance, the true separation of these terms is difficult to achieve because of hidden trade-offs. For example, special care must be taken to select recording sites at a large range of hypocentral distances, so that undesirable trade-offs between an event source term and the distance function are

avoided. Constraints must also be applied to reduce the number of degrees of freedom of the system, and to permit a stable inversion:

- $D(r=r_{ref},f) = 0$ at some reference distance. The reference distance, r_{ref}, used in the constraint is chosen such that errors in source depth at that distance would make little difference. Moreover, convenience suggests that supercritical reflections from the Moho in the continental crust should not appear in the chosen distance range.
- An additional reduction of the degrees of freedom of the system is achieved by forcing the summation of some (at least one), or all, the site terms to a null value: $\Sigma_i \ SITE_i = 0$. A side effect of this constraint is that anytime the absolute average would be nonzero, its value is automatically forced into all individual excitation terms. Site terms thus represent relative responses to the (sub) network average.

Once again, we emphasize the fact that we are not defining the earthquake source spectra; we are in fact parameterizing the observed ground motions.

Investigations by Atkinson (1993), Atkinson and Boore (1995) in eastern North America and by Atkinson and Silva (1997) in California indicate that the distance dependence of geometrical spreading may not have a simple functional form. However, in a log log space, the geometrical spreading may be expressed as a hinged, piecewise continuous, linear relation. Some requirements are forced on the geometrical spreading function, g (r), which should not differ significantly from r^{-1} at short distances (body-wave-like spreading), and should be close to $r^{-1/2}$ at larger distances (surface-wave-like spreading). Anderson and Lei (1994) and Harmsen (1997) extended the concept of describing a complex geometrical spreading function by fitting their data with many linear segments

(in a linear space), hinged and tied together with a smoothness constraint. With such an approach, the definitions of the geometrical spreading function, and of the frequency dependent Q is deferred to a later stage. At any given frequency, we parameterize the crustal propagation function as piecewise linear:

$$D(r, r_{ref}, f) = \sum_{i=0}^{n} L_i(r) D_i$$
$$D_{i=iref} = 0 \qquad (3)$$

where L_i (r) is a linear interpolation function, and the D_i are node values such that $D(r_i) = D_i$. A smoothness constraint can be applied by requiring

$$D_{i-1} - 2D_i + D_{i+1} = 0 \qquad (4)$$

A constraint to minimize roughness is easily incorporated in the system. If the nodes are evenly spaced, the constraint is effectively a minimum roughness one.

Given the level of ground motion at r_{ref}=40 km, D (r, r_{rref}, f) propagates the motion to the desired distance, r, and the site term adjusts the motion to a particular physical location (station). Other aspects of the parameterization that must be understood are the tradeoffs between excitation, site, and distance terms. Two cases illustrate the problem. First, if one event dominates a distance range, then there will be a tradeoff between the excitation for that event and the adjacent distance terms at that specific distance. This scenario may occur when an event is separated by a network dimension from a neighboring event, and if the distribution of distance nodes is too dense. A second case occurs if only one station dominates in a narrow range of distances, with an anomalous response. In this case, D(r, r_{ref}, f) will be distorted by this station, and a bias will be introduced in all other site terms by the site term constrains (Herrmann, 2000).

Data Analysis

The following procedure was followed in order to study the excitation and propagation of the ground motion:

1. Each waveform was first bandpass-filtered about a center frequency, f_c , by an 8-pole high-pass causal Butterworth filter with corner frequency at ($f_c/\sqrt{2}$) Hz, followed by an 8-pole low-pass Butterworth filter with corner frequency at $\sqrt{2}\ f_c$ Hz. The set of central frequencies was {0.5, 1, 2, 3, 4, 6, 8, 10, 12, 14, 16} Hz. The peak filtered ground velocity was saved.
2. In addition, a duration window was computed for each filtered time history. We used the 5% and 75% bounds of the normalized integral of the squared signal, following the S-wave arrival. For each central frequency, for each waveform, the unfiltered signal within this time window was Fourier transformed, and an rms-average of the Fourier velocity spectra was made between the two corners of the bandpass filter.
3. For each filter frequency, the peak filtered motion, Fourier velocity spectrum, duration and amplitudes of signal envelopes, were tabulated for use in later processing. The reason for saving this information for subsequent use of RVT (Boore, 1983), which relates rms-averaged spectral amplitudes and duration to peak motion.
4. The crustal propagation function, $D(r) = log_{10}\ (r, r_{ref}, f)$ was parameterized as a piecewise linear function with 14 nodes between 10 and 200 km. For our regression, we chose r_{ref} = 40 km. For each central frequency, there were 462 event terms, 159 site terms for the 53 three-component stations, and 14 nodes in

the distance function. The source-receiver distance distribution for the whole dataset is shown in Fig. 4. The range hypocentral distances spanned by our data set is evenly sampled by our observations, a characteristic that allows a stable inversion. The 14 nodal distances were chosen after looking at the data distribution.

5. A hybrid approach was used to perform the regressions: because of the presence of significant outliers, an L_1-norm inversion scheme (Bartels and Conn, 1980) was used to obtain the regression parameters. An L_2-norm regression scheme (SVD) was then used to obtain estimates of the standard errors. Given the large amount of data used, even though the hybrid approach is not rigorously correct (no assumptions are made on the statistical distribution of the residuals prior to the computation of the parameters), for any practical purposes, at least in the cases described in this study, the L_1- and the L_2-norm solutions (mean and median values) coincide when the distribution of the residuals is well-behaved. The L_1-norm procedure, however, protects us against severe individual deviations from the average behavior due to noisy individual data (for the time-domain quantities: spikes in the original time histories, and glitches induced by the action of the filters; for the frequency-domain quantities: wrong estimates of the rms-averaged Fourier spectral amplitudes due to substantial miscalculations of the 5-75% time window lengths. The standard errors associated to each parameter, although the distribution of the residuals is not perfectly Gaussian, may give idea of their scatter around the medians.

Results and Ground Motion Parameterization

Fig. 5 shows durations computed over all the available recordings, plots are shown for 6 of the central frequencies. An empirical function is calculated by using the L_1-norm inversion procedure, where the summation of the absolute values of residuals is minimized. We note significant scatter at 1.0 Hz, which substantially decreases at higher frequencies. Error bars are estimated using the L_2 norm. At higher frequencies, low signals due to attenuation did not permit a reliable estimation of duration at large distance.

The duration function is parameterized as a piecewise linear function of distance: $T(r) = \Sigma\, T_l N_l(r)$. No constraints are forced to the duration function, except T(r=0km) = 0, which is appropriate for small earthquakes. To determine the T(r) duration function, we assume the measured duration is practically insensitive to the event size for small earthquakes. RVT predictions depend on the assumed signal duration: T_s+T(r), where T_s is the source contribution and T(r) is the distance dependent wave propagation contribution (dispersion) to total duration. Predictions for larger earthquakes need extended source durations, T_s, to overcome the null duration constraint at short distance (Herrmann, 1985). The least squares fits are also plotted in Fig. 5.

The last stage of the processing entails the specification of a simpler parametric model to describe the observations. The Fourier velocity spectra, a(f,r), given the frequency and the hypocentral distance, are modeled as:

$$A(f, r) = s(f)\, g(r) \exp(-\pi f r / Q(f) \beta) \langle \nu(f) \exp(-\pi \kappa_o f) \rangle_{avg} \qquad (5)$$

where s(f) is the source spectrum term to generate ground velocity, g(r) is geometrical spreading, $Q(f) = Q_o (f / f_{ref})^n$ is the frequency-dependent propagation Q, β is the velocity of the S-waves, and the $\langle \nu(f) \exp(-\pi \kappa_o f) \rangle_{avg}$ term controls the average site

modification of the signal spectrum. ν(f) represents the site amplification term relative to generic "rock", similar to that of Atkinson and Silva (2000) for California. It can be computed from the shallow shear-wave velocity structure near the site (Boore, 1986). κ_o describes the depletion of high-frequency motion at the site, which may be due to the local Q(z) structure.

Figs 6a,b and 7a,b (colored lines) show the *D(r)* functions, empirically determined in the inversion as a function of frequency, for PGVs and Fourier amplitudes, together with the difference between the observed and predicted *D(r)* as a function of distance, respectively. As seen in Figs 6b and 7b, we successfully parameterize the distance effect, within ±0.1 log10 units in the first 100 km distance range. To enhance presentation, these figures show the deviation from an r^{-1} trend. Black lines in the background represent theoretical, RVT-based, predictions, obtained after a trial-and-error modeling obtained through the functional form:

$$10^{D(r_{ij}, r_{ref}, f)} = [g(r_{ij}) / g(r_{ref})] \exp[-\pi f (r_{ij} - r_{ref}) / Q(f) \beta] \quad . (6)$$

The functions (6) are deduced from the data through a trial-and error modeling procedure, where the Fourier amplitudes are produced in the entire distance range using an arbitrary source spectral model, and the geometrical/anelastic attenuation model described in (6). The forward model is solved at each frequency, after fixing the corresponding duration function to the values obtained from the regressions. All frequencies are simultaneously fitted by the frequency-dependent attenuation/duration model. Normalization to the arbitrary reference distance removes the effects of the specific source model and parameters used.

This is done by assuming $Q(f)=Q_o f^n$ and a simple piecewise linear geometrical spreading function. In our case, the functional form $g(r)$ used to fit the empirical results is:

$$
\begin{aligned}
f < 1 \text{ Hz}, \; g(r) &= r^{-1.2} \quad \text{for} \quad r \leq 30 \text{ km} \\
&= r^{-0.7} \quad \text{for} \quad 30 < r \leq 60 \text{ km} \\
&= r^{-1.4} \quad \text{for} \quad 60 < r \leq 100 \text{ km} \\
&= r^{-0.1} \quad \text{for} \quad r > 100 \text{ km}
\end{aligned}
$$

$$
\begin{aligned}
f \geq 1 \text{ Hz}, \; g(r) &= r^{-1.0} \quad \text{for} \quad r \leq 30 \text{ km} \\
&= r^{-0.6} \quad \text{for} \quad 30 < r \leq 60 \text{ km} \\
&= r^{-0.9} \quad \text{for} \quad 60 < r \leq 90 \text{ km} \\
&= r^{-0.1} \quad \text{for} \quad r > 100 \text{ km}
\end{aligned}
$$

The effect of anelastic attenuation is to reduce amplitude with distance by a factor of $exp\,(-\pi f r/ Q(f)\beta)$ where $\beta = 3.5$ km/sec. For the set of attenuation parameters Q_o, n and $g(r)$, theoretical Fourier spectra were estimated at each of the distances used in the regression for $D(r)$. Results were normalized to the reference distance of 40 km, and the logarithms were taken for direct comparison with the regression results. As a check, we also compared the $D(r)$ values obtained from the time domain regression by making random vibration theory estimates of peak filtered ground velocities. In doing so, we used the observed durations and random vibration theory (Boore, 1983). We accounted for the time domain response of the filters in the manner of Boore and Joyner (1984) for lightly damped single degree of freedom oscillators by stating that the RMS duration is the sum of the source duration, the propagation duration and twice the filter period. In addition, the duration used for determining the number of random peaks is the sum of the source duration, the propagation duration, and filter period. This exercise yielded $r_{ref} = 40$ km, $Q_o = 180$ and $n = 0.45$.

Figs 8 and 9 show the site terms from the regression on filtered peak amplitudes and Fourier velocity spectra. In general, the site terms for the radial and the transverse

components overlay. Because the constraint of null average was applied to the horizontal component site terms at the sites of the broadband stations, we may interpret the excitation terms of equation (2) as the horizontal ground motion that would be observed at the average network site, 40 km away from the hypocenter. Because of the averaging action introduction by regressing data from different azimuths, only the average source radiation pattern would be included.

The site terms are similar for the regressions in both the time and the frequency domains. Each term may be written as follows:

$$10^{SITEi\,(f)} = [\nu_i\,(f)\,\exp\,(-\pi\,\kappa_i\,f)] \,/\, <\nu(f)\,\exp(-\pi\,\kappa_o\,f)>_{avg} \qquad (7)$$

where the subscript *i* indicates the *i-th* site; $<\nu(f)\,\exp(-\pi\,\kappa_o\,f)>_{avg}$ is the average network site effect and $\nu(f)$ is the generic site amplification factor relative to generic "rock" site.

Finally, we compared the observed excitation levels of the horizontal motion for both data sets (peak values and Fourier spectra) at 40 km to model based predictions as a function of moment magnitude. Since there are data for $M_w > 5.0$ in our dataset, we felt confident in defining a source excitation model. The excitation spectra of especially larger events were modeled by using the regional propagation, together with the 2-corner equivalent-point–source model of Atkinson and Silva (2000) and a single-corner frequency Brune spectral model. The model for the horizontal velocity spectra is given by:

$$10^{EXC(r_{ref},\,f)} \approx C\,(2\pi f)\,M_o\,s\,(f)\,g\,(r_{ref})\,\exp\,(-\pi\,f\,r_{ref}/\,Q\,(f)\,\beta\,)\,\exp(-\pi\,\kappa_{eff}\,f) \quad (8)$$

where:

$$\exp(-\pi\kappa_{eff} f) \cong < \nu_i(f) \exp(-\pi\kappa_o f)>_{avg}$$

is the average high-frequency attenuation term due to the shallow geology,

$$C = (0.55)\ (0.707)\ (2.0)/\ 4\ \pi\ \rho\ \beta^3$$

and for the single-corner Brune model, the functional form for s (f) is given:

$$s(f) = 1 / (1 + (f / f_c) \qquad (9)$$

where $f_c = 4.9 * 10^6\ \beta\ (\Delta\sigma / M_o)^{1/3}$, corner frequency and the 0.55 represents the S-wave average radiation pattern, 2.0 is the amplification at the free surface, 0.707 is the reduction factor that accounts for the partitioning of energy into two horizontal components (Boore, 1983), ρ=2.8 g/cm^3 and β=3.5 km/sec are the density and the shear-wave velocity. The seismic moment is M_o.

Atkinson and Silva (2000) described their two-corner source spectral model as:

$$s(f) = [(1-\varepsilon) / [\ 1 + (f / f_a)^2\ ] + \varepsilon / [\ 1 + (f / f_b)^2\ ] \qquad (10)$$

where $\log f_a = 2.181 - 0.496$ M is the lower corner frequency, and $\log f_b = 2.41 - 0.408$ M is the higher corner frequency, is the frequency at which the spectrum attains ½ of the high-frequency amplitude level. The remaining parameter, $\log \varepsilon = 0.605 - 0.255$ M, is a relative weighting parameter whose value lies between 0 and 1.

Figs 10 and 11 compare the excitation terms at 40 km from our regressions for both the peak values and the Fourier spectral amplitudes with the predictions based on the Atkinson and Silva (2000), two corner source model combined with our crustal attenuation model and duration functions between 0.4 - 15 Hz. The gray curves in Figs 10 and 11 represent the theoretical excitation terms that are computed by using the parameters of Table 1.

In order to improve the presentation we first only plot error bars for the nine large events for which we have the seismic moments (M_w's), with the predictions based on the two source models (one-corner Brune, 1970 and two-corner, Atkinson and Silva, 2000, source model), respectively, in Figures 12a,b. The excitation spectra of larger events were modeled by using the regional propagation, a single-corner frequency Brune spectral model (Brune, 1970, 1971) characterized by an effective stress parameter, $\Delta\sigma$=80 bar (Fig 12a), and by a regional estimate of the near-surface, distance-independent, network averaged attenuation parameter, κ_0=0.055 sec that was estimated from the roll-off the empirical source spectra obtained from the regressions (Table 2).

The model fits the observation of the large earthquakes, the M_w=6 fits close to the mean of the M_w 5.7-5.9 events, some adjustment at high frequencies may be required for M_w=5.0 events, but this adjustment is not that important if one is really interested in the big earthquake motions. The predicted shapes and levels are within the error bounds for the M_w ~ 5.0 earthquakes. The fit for larger earthquakes is excellent for frequencies greater than or equal to 2 Hz. The fit at high frequencies means that we would have confidence in using this model to predict peak accelerations. Concerning the fit at M_w 5.7-5.9, we have two earthquakes that are fitted very well with the Atkinson and Silva (2000) source model. The M_w=6.0 prediction at frequencies greater than 5 Hz goes through the mean of the levels of the M_w 5.7 and 5.9. Even though we have many stations that should average over the radiation pattern, these events behave very differently at high frequencies, which reinforces the idea that earthquake of the same size can radiate energy in different fashions. Fits to the M_w=7.2 are very similar for both models, the

Atkinson and Silva (2000) one is slightly better at the low frequencies. Both models do not work well for the M_w=6.0 and underestimate high frequency levels for M_w = 5.0.

Fig. 13 shows the residuals in fitting the log a (f, r) with equation (2); the scatter is typical of such regressions.

Empirical Predictive Attenuation relationships

Stochastic point-source simulations using the two-corner source spectrum of Atkinson and Silva (2000) were used to predict the absolute levels of ground shaking. In doing so, we followed Boore's (1996) implementation (Boore's SMSIM code), and used the attenuation parameters and the empirical duration function, obtained in this study. We compare these values to the peak ground acceleration observations of the 17 August 1999, Izmit earthquake and several attenuation relationships for the California and the Western U. S. The reason for using this earthquake, instead of main-shock of the 12 November, 1999, M_w=7.2 Duzce earthquake, is that there were many more observations at the closest distance. The fact permits us to test our predicted relationships. Fig. 14 shows a comparison between the attenuation relations by Ozbey *et al*., (2004, OZB04), Boore *et al*., (1997, BJF97), Atkinson and Silva, (2000, AS2000) and our results obtained for the BC site conditions (soil classification of the U.S. National Earthquake Hazard Research Program, NEHRP), (Boore and Joyner, 1997) for PSA at frequencies of 1 Hz, 3 Hz and 5 Hz. This site condition is the boundary between NEHRP classes B and C, (i.e, a site with an average shear wave velocity - V_s - of 760 m/sec in the top 30m). This refers to site as "firm rock," differentiating it from "hard rock" with shear-wave velocities near 3.0 km/sec at the surface.

The OZB04 attenuation relationship was obtained from strong motion records, from stations operated by the Bogazici University, the Kandilli Observatory and the Earthquake Research Institute (KOERI), by Istanbul Technical University (ITU), and by the General Directorate of Disaster Affairs' Earthquake Research Department (ERD). Their cumulative data set consisted of 195 records from 17 earthquakes with $M_w \geq 5.0$. The BJF97 relationship was calibrated using strong motion records for shallow earthquakes in western North America, and cannot be used to predict ground motions at distances greater than 80 km, or for magnitudes less than 5.5 or greater than 7.5. The AS2000 attenuation relationships have been developed for California based on a stochastic model, which combines the main advantages of both point-source and finite-fault modeling approaches. The stochastic ground motion relationships are underpinned by a source model that has been validated for earthquakes from magnitudes 4 through 8. Their attenuation model is derived from regional seismographic data over distances of hundreds of km (Raoof et al., 1999).

The predicted spectral accelerations of this study are very similar to those by BJF97, over the entire distance range at 3 and 5 Hz, but there are significant differences at short distances. With respect to our predictive relationships, AS2000 and OZB04 show higher and lower amplitudes, respectively, over almost the entire distance range and especially at 3 and 5 Hz. Our predicted results are in good agreement with BJF9's and AS2000's ones, in the distance range 10-200 km, at frequencies of 1.0 Hz, and they are always higher than OZB04's ones. Even though we used $g(r)= r^{-0.1}$, which is different from $g(r)= r^{-0.5}$, used for existing strong-motion predictive relationships (for Europe,

California, Western U.S and other active tectonic regions) beyond 100 km, our empirical relationship is in good agreement with BJF9's, AS2000's and OZB04's ones.

Conclusions and Discussion

Using ground velocities from three-component recordings from the Marmara region, we have characterized the ground velocity distance scaling in the range 10 - 200 km. Results of this study indicate that low frequency signals have longer durations than high frequency ones, and that duration increases significantly with distance. The low frequency duration data exhibit much scatter up to 1.0 Hz. Duration results indicate that both the degree of distance dependence and scatter increase with decreasing frequency.

The empirical distance and site terms obtained from the Fourier amplitude and from the time domain data are similar. Random Vibration Theory (RVT) has been used to model the observed peak ground motion. Peak velocities are controlled by a combination of source characteristics, duration of the signal, geometrical spreading, and anelastic attenuation. Results from the application of RVT indicate that our data are well fitted with a hinged, quadri-linear geometrical spreading function. We propose a frequency-dependent quality factor $Q(f) = 180 f^{0.45}$ for the combined three-component data set. We find that the amplitude of high-frequency ground motion in the Marmara region decreases rapidly $g(r) = r^{-1.2}$ at short distances ($r < 30$) and low frequencies ($f < 2$ Hz). The observed decay is stronger than what is observed in other settings studied using the same technique: Central Europe (Malagnini *et al*., 2000a), the Apennines region of Italy (Malagnini *et al*., 2000b), the Friuli region of northeastern Italy (Malagnini *et al*., 2002), southern California (Raoof *et al*, 1999) and Utah (Jeon, 2000). This rapid decrease has implications for ground motion predictions for large earthquakes. For longer distances

(beyond 60-70 km) the interaction between seismic waves and propagation medium is more complex, as suggested by a geometrical spreading coefficient $r^{-0.9}$ for 60-100 km distances and $r^{-0.1}$ for distances R>100 km. Researchers often pre-define the functional dependence of g(r) for the region of interest, requiring $r^{-1.0}$ at short distances for body waves and $r^{-0.5}$ at larger distances for surface waves. The exponents of the geometrical spreading function describe the geometry of the wave-front (e.g., spherical or cylindrical propagation, or even the appearance of supercritical reflections in the transitional distance ranges), which strongly depends on the velocity structure of the medium (Aki and Richards, 2002). It is clear that if we fix the geometrical spreading function to 1/*r,* we hypothesize a spherical wave front, and hence, implicitly, a uniform crust. For a detailed estimate of the nature of the geometrical spreading, we need to take into account possible crustal heterogeneities and the existence of a strongly layered structure (e.g., the existence of a strong discontinuity, the Moho). Our g(r) results differ from $r^{-0.5}$ at relatively long distances. This could be caused by the boundary between the falloff of direct wave, the emergence of lower crustal or Moho reflections and the contribution of the SmS phases. The overall behavior depends on several factors, such as: focal depth, crustal thickness, crustal velocity gradient, etc. Differences are seen in the geometrical spreading functions in our study at low and high frequencies might be also responsible for a laminated lower crust or a thick crust-mantle transition zone. In fact, Boztepe-Guney and Horasan (2002) observed the large amplitude SmS phases arrive 2 to 3 sec after direct S-waves in the distance range between 120 and 160 km. The amplitude of SmS arrivals is 3-6 times larger than the amplitude of the direct S-waves. These results suggest that the crust may not have a simple structure in the Marmara Sea, and that the

effect of the large-amplitude SmS phases on the ground motion should be taken into consideration in the studies related with the seismic hazard in the region (Boztepe-Guney and Horasan, 2002).

This study improves the estimate of the frequency-dependent crustal attenuation of the region over what was previously available. Gunduz et al. (1998) estimated $Q_c(f)=41f^{1.08}$ and $Q_s(f)=50f^{1.09}$ in the Marmara region, in the distance range between 20 and110 km, and in the frequency range between 1.5 and 24 Hz. Akyol et al, (2002) found $Q_s(f)=47f^{0.67}$ around the Bursa area (eastern part of the Marmara region). The frequency dependence suggested by Gunduz et al, (1998) seems to be extremely high when compared with other results from Mediterranean regions, California, or the western United States. Raoof et al., (1999) determined that the California attenuation can be modeled by geometrical spreading of r^{-1} to a distance of 40 km, with $r^{-0.5}$ spreading for r greater than 40 km. The anelastic attenuation associated with this spreading model is presented by a frequency-dependent regional quality factor given by $Q_s(f)=180f^{0.42}$. Jeon (2000) estimated the attenuation function to be between $Q_s(f)=145f^{0.65}$ and $Q_s(f)=180f^{0.60}$ for Utah (Basin and Range Province). Baskoutas et al, (2000) found $Q_s(f)=108f^{0.65}$ for 40 s lapse time window at the Erythres station, in the central Greece.

The fact that a single functional form for Q(f) is used for all distances is somehow inappropriate because the direct radiation recorded at short distances mainly samples the crust above the hypocenter, whereas at large distances the seismic waves sample the entire crust. Therefore, the used method loses any azimuthal or depth information contained in each recording, yielding a picture of the statistical characteristics of the crustal-wave propagation in the region.

The estimated κ_{eff} = 0.055 sec value is consistent with the average value of κ=0.056 sec found by Durukal and Catalyurekli (204) in the northwestern Turkey for the sites belonging to class D of the NEHRP soil classification (Boore and Joyner, 1997).

A comparison of the Fourier domain excitation terms (Fig. 10) and the time domain terms (Fig. 11) shows the same relative pattern between data and predictions. This supports the internal consistency of our parameterization of the data in terms of anelastic attenuation, geometrical spreading and duration. Especially at the low frequencies, a spectral model characterized by two corner frequencies fits better the observed excitation terms for large events in Marmara than does a single-corner frequency Brune spectrum (Fig 12a, b).

As an exercise in ground motion prediction, we used the model parameters of Table 1 and a set of programs called SMSIM (Stochastic Model SIMulation, Boore, 1966), to predict expected peak spectral accelerations (PSA). Since we have more PGA observations than for the 7.2, Duzce earthquake for closest distances, we compare our predicted values to the PGA's observed during the August 17, 1999 (M_w = 7.4) event, and used the predictions of the OZB97, AS2000 and BJF97 models. Compared to their predicted PSA's, our model is in good agreement with BJF97, and it yields higher and lower values than, respectively, the AS2000's and OZB97's ones, between a distance range of 10-100 km. This is especially true at 3 and 5 Hz.

We have shown the value of using aftershock recordings to describe the characteristics of the high-frequency ground motions as a function of hypocentral distance. When calibrated over large aftershocks with known seismic moment, the technique can provide excellent estimates of expected high frequency ground motion from large earthquakes.

References

Ambraseys, N, N., 1970. Some characteristic features of the Anatolian fault zone. *Tectonophysics*, 9, 65-143.

Ambraseys, N, N., 1975. Studies in historical seismicity and tectonics, *Geodynamics Today*, Royal Soc. Publ., London.

Ambraseys, N. N., K. A. Simpson and J .J. Bommer, 1996 Prediction of Horizontal Response Spectra in Europe. *Earthquake Engineering and Structural Dynamics*, 25, 371-400.

Anderson, J. G., and Y. Lei 1994. Nonparametric description of peak acceleration as a function of magnitude, distance, and site in Guerrero, Mexico, *Bull. Seis. Soc. Am*. 84, 1003-1017.

Aki, K., Richards, P., 2002. Quantitative Seismology, 2nd ed. University Science Books, Sausalito, CA. 700 pp.

Akinci, A., Malagnini, L., Herrmann, R.B, Pino, N.A., Scognamiglio, L., Eyidogan, H., 2001. High-Frequency Ground Motion in the Erzincan Region, Turkey: Inferences from Small Earthquakes, *Bull. Seis. Soc. Am.,*91, 6, 1446-1455.

Akyol, N., Akinci, A., Eyidogan, H, 2002. Separation of Source, Propagation and Site Effects from Observed S-wave of Bursa City and Its Vicinity in the North-western Anatolian Fault Zone, Turkey, *Pure and Applied Geophysics*, Volume 159, Number 6, pp 1253-1269.

Atkinson, G. M. 1993. Earthquake source spectra and attenuation in southeastern Canada, University of Western Ontario, London, Ontario, *Ph.D. thesis*.

Atkinson, G. M., and D. M. Boore 1995. Ground-motion relations for eastern North America, *Bull. Seism. Soc. Am.,* 85, 17-30.

Atkinson, G. M., and W. Silva 1997. An Empirical study of earthquake source spectra for California earthquakes, *Bull. Seism. Soc. Am.,* 87, 97-113.

Atkinson, G. M., and W. Silva, 2000. Stochastic Modeling of California Ground Motion. *Bull. Seism. Soc. Am.,* 90, 255-274.

Barka, A., 1992. The North Anatolian Fault Zone. *Annales Tetonicae, Suppl*. To Vol. VI: 164-195.

Barka, A. A., 1996. Slip distribution along the North Anatolian fault associated with the large earthquakes of the priod 1939- to 1967. BSSA, 86, 5, 1238-1254.

Barka, A. A., 1997. Neotectonics of the Marmara Region. *Active tectonics of Northwestern Anatolia-The Marmara Project*. Ed., C. Schindler and M. Pfister. VDF, ETH Zurich. 55-88.

Bartels, R.H. and Conn, A. R., 1980. Linearly constrained discrete L_{-1} problems, *Transactions of the ACM on Mathematical Software*, vol. 6(4), pp. 594-608.

Baskoutas I., G. Panopoulou and Th. Rontoyanni, 2000. The seismic attenuation in two regions with different geological aspect. *Boll. Geof. Theor. Appl*., Vol 41, No3 pp233-242.

Bodin, P., L. Malagnini, and A. Akinci, 2004. Ground-Motion Scaling in the Kachchh Basin, India, Deduced from Aftershocks of the 2001 M_w 7.6 Bhuj Earthquake, *Bull. Seism. Soc. Am.,* 94, 5, 1658-1669.

Boore, D. M. 1983. Stochastic simulation of high-frequency ground motions based on seismological models of the radiated spectra, *Bull. Seism. Soc. Am.,* 73, 1865-1894.

Boore, D. M., and W. B. Joyner 1984. A Note on the Use of Random Vibration Theory to predict peak amplitudes of transient signals, Letter to the Editor, *Bull. Seism. Soc. Am.,* 74, 2035-2039.

Boore, D. M. 1986. Short-period P- and S-wave radiation from large earthquakes: implications for spectral scaling relations*. Bull. Seism. Soc. Am*., 76, 43-64.

Boore, D. M., and W. B. Joyner 1991. Estimation of ground motion at deep-soil sites in eastern North America*, Bull. Seism. Soc. Am.,* 81, 2167-2185.

Boore, D. M., 1996. SMSIM-Fortran programs for simulating ground motion from earthquakes: version 1.0, *U. S. Geological Survey open-file report* 96-80-A, 73 p.

Boore, D. M. and W. B. Joyner, 1997. Site amplifications for generic rock sites. *Bull. Seism. Soc. Am.,* 87, 327-341.

Boore, D. M., W. B. Joyner and T. E. Fumal, 1997. Equations for Estimating Horizontal Response Spectra and Peak Acceleration from Western North American Earthquakes: A summary of Recent Work. *Seism. Res. Lett.*, 68, 1, 128-153.

Boztepe-Güney, A., Horasan, G., 2002. Enhanced ground motions due to large-amplitude critical reflections (SmS) in the Sea of Marmara, *Geophysical Research Letters,* 29, 9-1/9-4.

Brune, J., 1970. Tectonic stress and the spectra of seismic shear waves from earthquakes. J. Geophys. Res. 75, 4997– 5009.

Campell, W., K., 1997. Empirical near-source attenuation relationships for horizontal and vertical components of peak ground acceleration, peak ground velocity, and pseudo-absolute acceleration response spectra. *Seis. Res. Lett.*, 68,1, pp.128-154.

Celebi M., S. Akkar, U. Gulerce, A.Sanli, H. Bundock, A. Salkin, 2001. Main shock and aftershock records of the 1999 Izmit and Duzce, Turkey earthquakes. USGS/OFDA project [USGS project no: 1-7460-63170]. http://geopubs.wr.usgs.gov/open-file/of01-163/

Durukal E., Y.Çatalyürekli, 2004. Spectral Analysis of Source Parameters of the 1999 Kocaeli and Düzce Earthquake Aftershock Sequences, *proceeding of the 13th World Conference on Earthquake Engineering,* Vancouver, Canada, 1-6 August 2004.

Gok, R. and L. Hutchings, 2006. Source Parameters and Scaling Relations for 1999 North Anatolian Fault Zone Aftershocks, in preparation.

Gunduz, H., K. Ayse, B. Aysun and T. Niyazi, 1998. S-wave attenuation in the Marmara region, northwestern Turkey, *Geophysical Research Letters*, *25*, 2733-2736.

Harmsen, S. 1997. Estimating the Diminution of Shear-Wave Amplitude with Distance: Application to the Los Angeles, California, Urban Area. *Bull. Seism. Soc. Am,.* 87, 888-903.

Herrmann, R. B. 2000. Comparative ground motion studies, USGS Award Number: 1434-HQ-97-GR03090. 80

Herrmann, R. B., 1985. An extension of Random Vibration Theory estimates of strong ground motion to large earthquakes, *Bull. Seis. Soc.Am.,* 75, 1447-1453.

Hubert-Ferrari, A., A. Barka, E. Jacques, S. S. Nalbant, B. Meyer, R. Armijo,P. Tapponier, and G.C.P. King, 2000. Seismic hazard in the Sea of Marmara following the Izmit earthquake. *Nature*, 404, 269-272.

Jeon, Y. S., 2000. High frequency earthquake ground motion scaling in Utah, *M.S. Thesis,* Saint Louis University.

Kramer, S. L., 1996. Geotechnical Earthquake Engineering, Prentice Hall.

Le Pichon, X., Sengor, A.M.C., Demirbag , E., Ragin, C., Imren, C., Armijo, R., Gorur, N., Catagay, N., Mercier de Lepinay, B., Meyer, B., Saatcilar, R., Tok, B., 2001. The active Main Marmara Fault. Earth Planet. Sci. Lett. 192, 595– 616.

McKenzie, D., 1972. Active tectonics of the Mediterranean region, *Geophys J. R. Astr. Soc.* 30, no. 2, 109–185.

Malagnini, L., R.B. Herrmann and K. Koch 2000a. Regional ground motion in scaling in Central Europe, *Bull. Seism. Soc. Am*. 90, 1052-1061.

Malagnini L., R. B. Herrmann and M. Di Bona 2000b. Ground motion scaling in the Apennines (Italy), *Bull. Seism. Soc. Am*., 90, 1062-1081.

Malagnini, L., Akinci, A., Herrmann, R. B., Pino, N.A., Scognamiglio, L, 2002. Characteristics of the ground motion in Northeastern Italy, *Bull. Seism. Soc. Am.,* 26, 2186-2204 .

Mayeda K., R. Gök, W. R. Walter, and A. Hofstetter, 2005. Evidence for Non-Constant Energy/Moment Scaling From Coda-Derived Source Spectra, *Geophysical Research Letter*, Vol. 32, L10306, doi:10.1029/2005GL022405.

Michel, G., 1994. Neo-kinematics along the North-Anatolian Fault (Turkey), PhD thesis, Tu¨binger geowiss. Arb., Reihe A 16.

Nalbant, S., Hubert, A. and King, G. C. P., 1998. Stress coupling between earthquakes in northwest Turkey and the north Aegean Sea., *Journal of Geophy. Res*., 103, B10, 24,469-24,486.

Neugebauer, J., Loffler, M., Berckhemer, H. and Yatman, A., 1997. Seismic observations at an overstep of the western North-Anatolian Fault (Abant-Sapanca region, Turkey), *Geol. Rund*., 86, 93–102.

Okay, A. I., Ozcan, A. K., Imren, C., Guney, A. B., Demirbag, E., Kuscu, I., 2000. Active faults and evolving strike–slip basins in the Marmara Sea, northwest Turkey: a multichannel seismic reflection study. Tectonophysics 321, 189–218.

Orgulu, G., Aktar, M. 2001. Regional Moment Tensor Inversion for Strong Aftershocks of the August 17, 1999 Izmit Earthquake (Mw=7.4), *Geophysical Research Letters*, 28, No. 2, 371-374.

Ozbey, C., Sari, A., Manuel, L., Erdik, M. Fahjan, Y., 2004. An empirical attenuation relationship for Northwestern Turkey ground motion using a random effects approach. *Soil Dynamics and Earthquake Engineering,* 24, 115–125

Parsons, T., 2000. Heightened odds of large earthquakes near Istanbul: An interaction-based probability calculation, *Science,* 288, 661–665.

Raoof, M., R. B. Herrmann, and Malagnini, L. 1999. Attenuation and excitation of three-component ground motion in Southern California, *Bull. Seism. Soc. Am*. 89, 888-902.

Sadigh, K. 1997. Attenuation relationships for shallow crustal earthquakes based on California strong motion data, *Seism. Res. Lett*., 68, No. 1, 180-189.

Stein, R. S., Barka, A. A. and Dietrich J. H., 1997. Progressive failure on the North Anatolian Fault since 1939 by earthquake stress triggering. *Geophy. J. Int*., 128, 594-604.

Straub, C., and Kahle, H. G., 1995. Active crustal deformation in the Marmara sea region, N. W. Anatolia, inferred from GPS measurements. *Geophs. Res. Lett*., 22, 18, 2'533-2'536.

Toro, G. R. and R. K. McGuire 1987. An investigation into earthquake ground motion characteristics in eastern north America, *Bull. Seism. Soc. Am*. 77, 468-489.

Sengor, A.M.C., Gorur, N. and Saroglu, F., 1985. Strike-slip faulting and related basin formation in zones of tectonic escape: Turkey as a case study. In: Strike- Slip Faulting and Basin Formation (K.T. Biddke and N. Christie-Blick, eds). Spec. Publ. Soc. Econ. Paleont. Miner., Tulsa, 37, 227–264.

The World Bank, Turkey, 1999. Marmara Earthquake Assessment, from the World Wide Web http://www.worldbank.org, September 14, 1999 and http://www.imf.org/external/NP/LOI/1999/092999.HTM.

Figure Captions

Figure 1. Strip map showing the 1500-km-long North Anatolian fault. Relatively straight, the fault has several short, minor strands associated with it along its eastern half and breaks into three strands to the west. The section of the fault that ruptured to the surface during the 1999 Izmit and Duzce earthquakes are shown with the dashed line. In 1999, the fault ruptured along the northernmost, generally east-west main strand, as well as along a northerly strand called the Düzce fault. Modified from Barka (1996).

Figure 2. Location of stations (solid triangles) and earthquakes (open circles) used for this study. The size of the circles indicates relative earthquake magnitudes.

Figure 3. Moment magnitude distribution of the records used for the regression analysis.

Figure 4. Source-receiver hypocentral distance distribution of data used for the regression analysis. The horizontal axis refers to hypocentral distance (km), whereas on the vertical axis shows the names of the seismic stations. Each small square corresponds to a single horizontal-component recording

Figure 5. Distance dependence of duration for 0.25, 0.40, 1.0, 3.0 and 5.0 Hz filtered data.

Figure 6. a) Colored curves show attenuation functional $D(r, r_{ref}, f)$ obtained from the regression the filtered velocities together with b) the difference between the observed and predicted *D(r)* as a function of distance at frequencies of 1.0, 2.0, 3.0, 4.0, 5.0, 6.0, 8.0, 10.0, 12.0, 14.0 and 16.0 Hz. Black lines in the background represent theoretical predictions obtained after a trial-and-error modeling of the empirical (color) curves. The

reference hypocentral distance is 40 km. Frequency dependence of filtered time domain D(r) corrected for r^{-1} geometrical spreading coefficient.

Figure 7. a) Colored curves show attenuation functional D(r, r_{ref}, f) obtained from the regression the Fourier amplitudes together with b) the difference between the observed and predicted *D(r)* as a function of distance at frequencies of 1.0, 2.0, 3.0, 4.0, 5.0, 6.0, 8.0, 10.0, 12.0, 14.0 and 16.0 Hz. Black lines in the background represent theoretical predictions obtained using trial-and-error modeling of the empirical (color) curves. The reference hypocentral distance is 40 km. Frequency dependence of Fourier velocity spectra D(r) corrected for r^{-1} geometrical spreading coefficient. b)

Figure 8. The site terms obtained from regression of Fourier velocity spectra.

Figure 9. The site terms obtained from regression horizontal peak filtered velocities.

Figure 10. Excitation of peak filtered velocity at a reference hypocentral distance r_{ref}=40 km. Excitation terms for all events used in this study with magnitude between M_w=2.5 and 7.2 are compared to predictions obtained by using RVT. The gray curves representing the theoretical source terms are computed for magnitudes of 3.0, 4.0 5.0, 6.0 and 7.2 by using the parameters of Table 1.

Figure 11. Excitation of Fourier velocity spectra at a reference hypocentral distance r_{ref}=40 km. Excitation terms for all events used in this study with magnitude between

M_w=2.5 and 7.2 are compared to predictions. The gray curves representing the theoretical source terms are computed for magnitudes of 3.0, 4.0 5.0, 6.0 and 7.2 by using the parameters of Table 1.

Figure 12. Excitation of peak filtered velocity at a reference hypocentral distance r_{ref}=40 km. Excitation terms for nine large events with the predictions based on the two source models, a) one-corner Brune, 1970 and b) two-corner, Atkinson and Silva, 2000, source model, for which we have the seismic moments, indicated with boxes (showing M_w) and arrows to the excitation, respectively. The gray curves representing the theoretical source terms are computed for magnitudes of 5.0, 6.0, 7.2 by using the parameters of Table 1 and Table 2.

Figure 13. The residuals of the regressions, for six of the sampling frequencies (1.0, 2.0, 4.0, 5.0, 10.0 and 16.0 Hz).

Figure 14. Comparison of different estimates of PSA (g) at frequencies of 1.0, 3.0 and 5.0 Hz in the Marmara region as obtained by using the empirical relationships by Ozbey *et al*., (2004, dotted), Boore *et al*., (1997, gray line) and Atkinson and Silva (2000, short dashed); dark solid line indicate PSA computed by Boore's program SMSIM (Boore, 1996) using the crustal attenuation and excitation parameters shown in Table 1. Curves are computed for M_w 7.4 and compared to the observed values of PGA (at soft, stiff and rock sites) during the 17 August 1999, M_w =7.4, Izmit earthquake.

Table 1.

High frequency ground motion model parameters

(two corner frequency source model)

$\rho = 2.8$ g/cm^3

$\beta = 3.5$ km/sec

$\kappa_{eff} = 0.055$ sec

$\log f_a = 2.181 - 0.496$

$\log f_b = 2.41 - 0.408\ M$

$\log \varepsilon = 0.605 - 0.255\ M$

$f < 1$ hz, $g(r) = r^{-1.2}$ for $r \leq 30$ km
$= r^{-0.7}$ for $30 < r \leq 60$ km
$= r^{-1.4}$ for $60 < r \leq 100$ km
$= r^{-0.1}$ for $r > 100$ km

$f \geq 1$ hz, $g(r) = r^{-1.0}$ for $r \leq 30$ km
$= r^{-0.6}$ for $30 < r \leq 60$ km
$= r^{-0.9}$ for $60 < r \leq 100$ km
$= r^{-0.1}$ for $r > 100$ km

$Q(f) = 180\ (f / 1.0)^{0.45}$

Table 2.

High frequency ground motion model parameters

(one-corner frequency source model)

$\rho = 2.8$ g/cm^3

$\beta = 3.5$ km/sec

$\kappa_{eff} = 0.055$ sec

$\Delta\sigma = 80$ bar

$f_a = f_b$

$f < 1$ Hz, $g(r) = r^{-1.2}$ for $r \leq 30$ km
$= r^{-0.7}$ for $30 < r \leq 60$ km
$= r^{-1.4}$ for $60 < r \leq 100$ km
$= r^{-0.1}$ for $r > 100$ km

$f \geq 1$ Hz, $g(r) = r^{-1.0}$ for $r \leq 30$ km
$= r^{-0.6}$ for $30 < r \leq 60$ km
$= r^{-0.9}$ for $60 < r \leq 100$ km
$= r^{-0.1}$ for $r > 100$ km

$$Q(f) = 180 \, (f / 1.0)^{0.45}$$

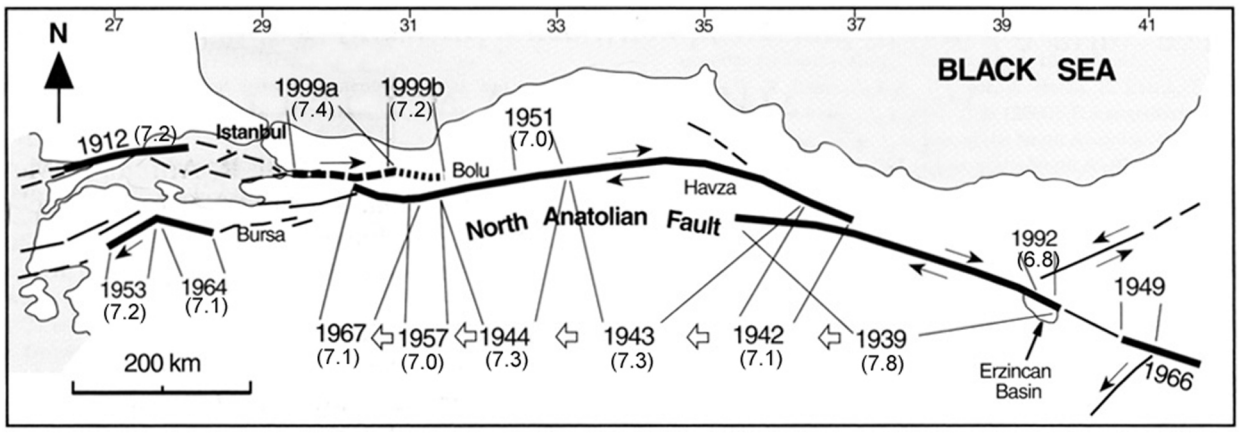
N
27
29
31
33
35
37
39
41
BLACK SEA
1999a
(7.4)
1999b
(7.2)
1912 (7.2)
Istanbul
1951
(7.0)
Bolu
Havza
North Anatolian Fault
Bursa
1992
(6.8)
1949
1953
(7.2)
1964
(7.1)
1967
(7.1)
1957
(7.0)
1944
(7.3)
1943
(7.3)
1942
(7.1)
1939
(7.8)
200 km
Erzincan
Basin
1966

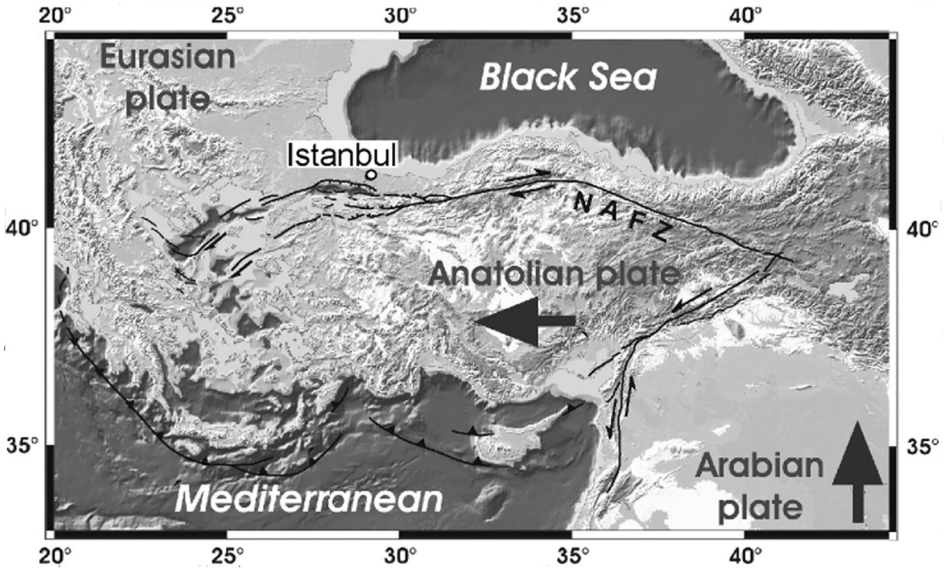
20°
25°
30°
35°
40°
Eurasian
plate
Black Sea
Istanbul
NAFZ
40°
Anatolian plate
35°
Arabian
plate
Mediterranean

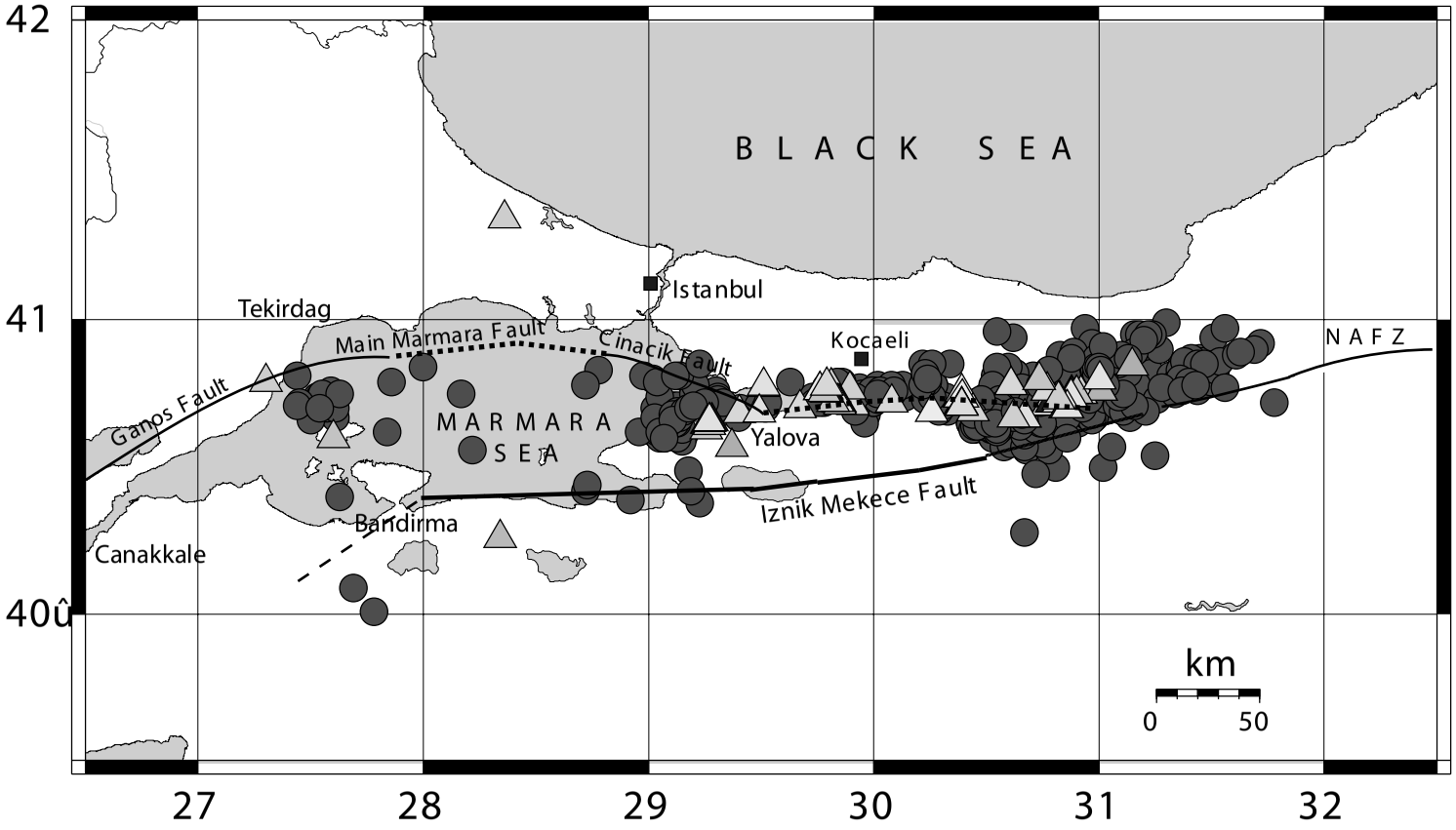
42
41
40û
27
28
29
30
31
32
BLACK SEA
Istanbul
Tekirdag
Main Marmara Fault
Cinacik Fault
Kocaeli
NAFZ
Ganos Fault
MARMARA
SEA
Yalova
Iznik Mekece Fault
Bandirma
Canakkale
km
0
50

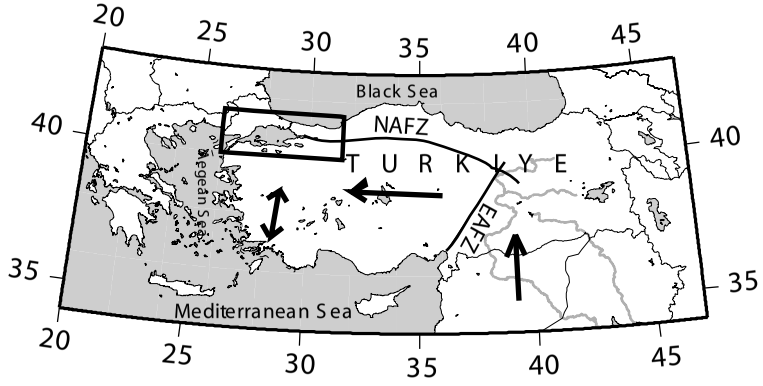
20
25
30
35
40
45
40
35
Black Sea
NAFZ
T U R K I Y E
Aegean Sea
EAFZ
Mediterranean Sea

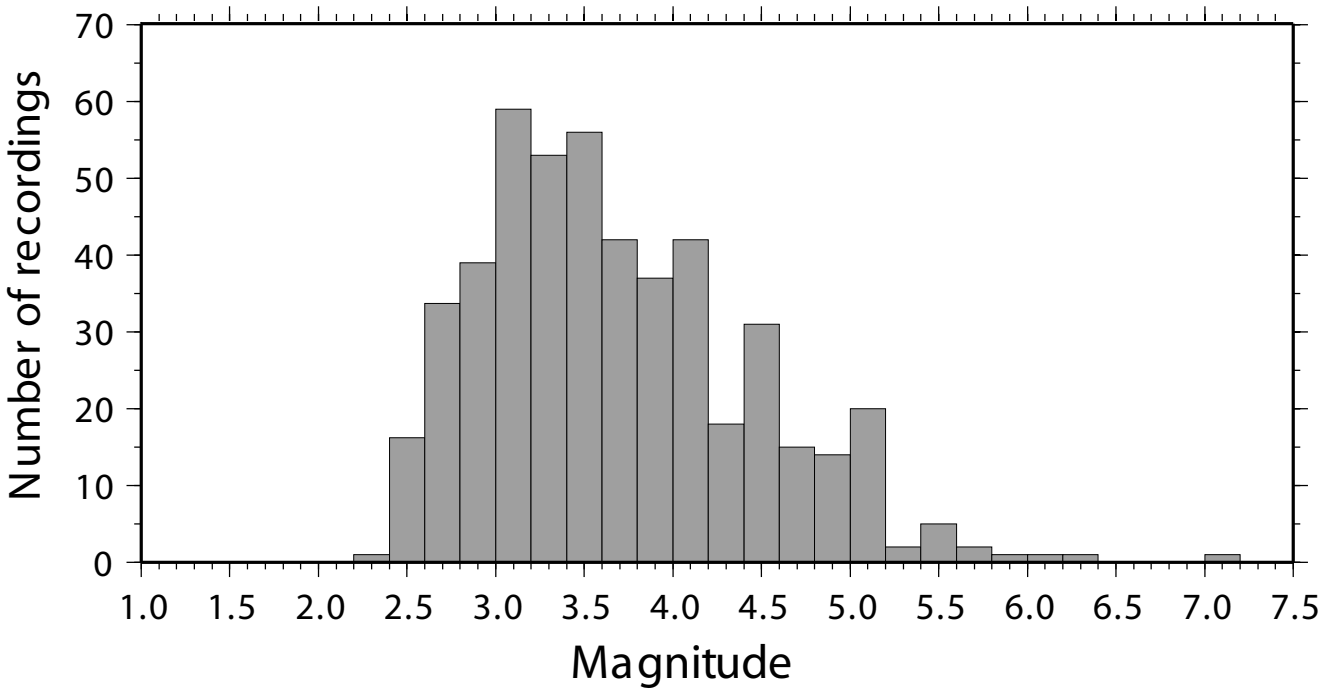
Number of recordings
70
60
50
40
30
20
10
0
1.0
1.5
2.0
2.5
3.0
3.5
4.0
4.5
5.0
5.5
6.0
6.5
7.0
7.5
Magnitude

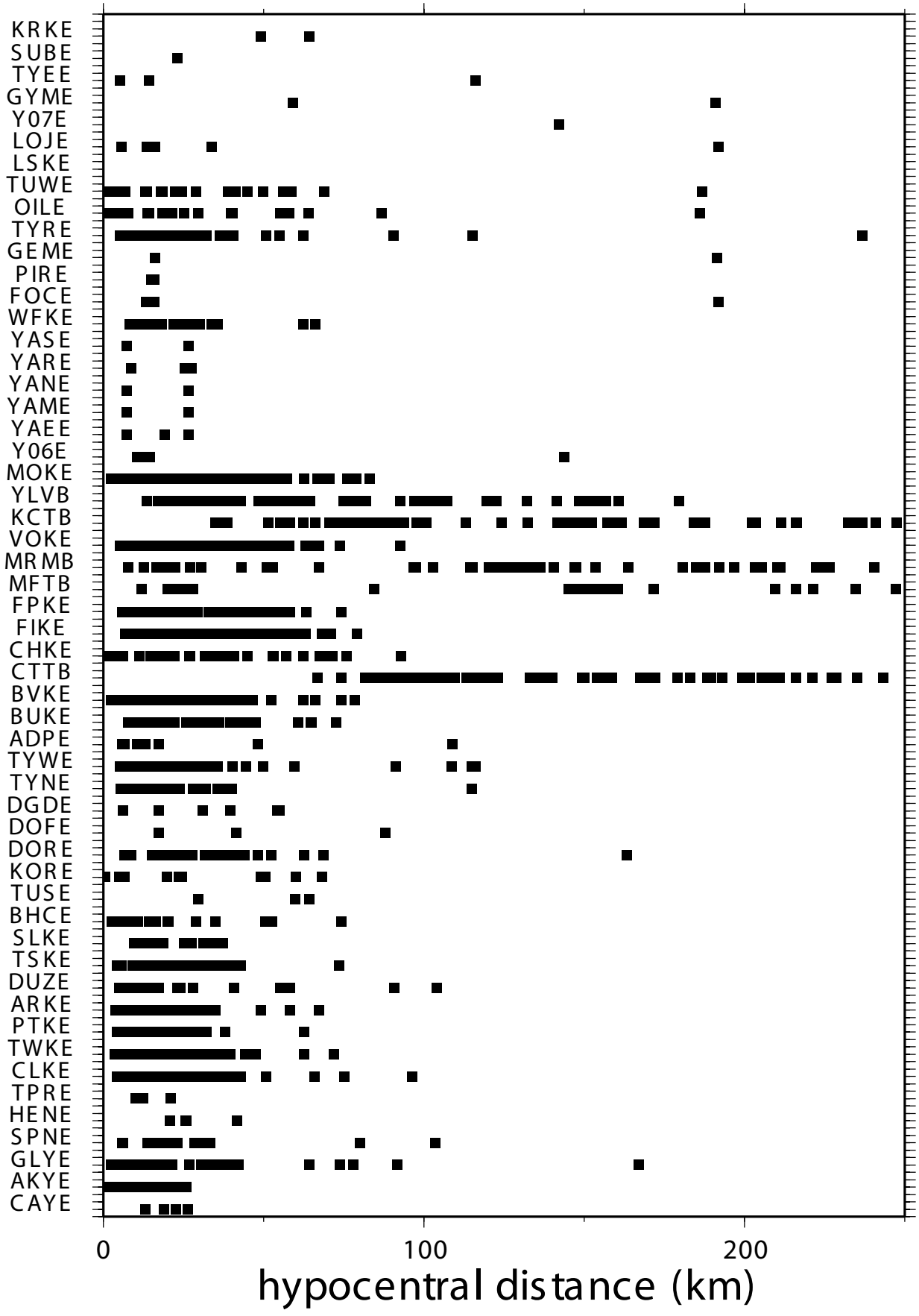
KRKE
SUBE
TYEE
GYME
Y07E
LOJE
LSKE
TUWE
OILE
TYRE
GEME
PIRE
FOCE
WFKE
YASE
YARE
YANE
YAME
YAEE
Y06E
MOKE
YLVB
KCTB
VOKE
MRMB
MFTB
FPKE
FIKE
CHKE
CTTB
BVKE
BUKE
ADPE
TYWE
TYNE
DGDE
DOFE
DORE
KORE
TUSE
BHCE
SLKE
TSKE
DUZE
ARKE
PTKE
TWKE
CLKE
TPRE
HENE
SPNE
GLYE
AKYE
CAYE
0
100
200
hypocentral distance (km)

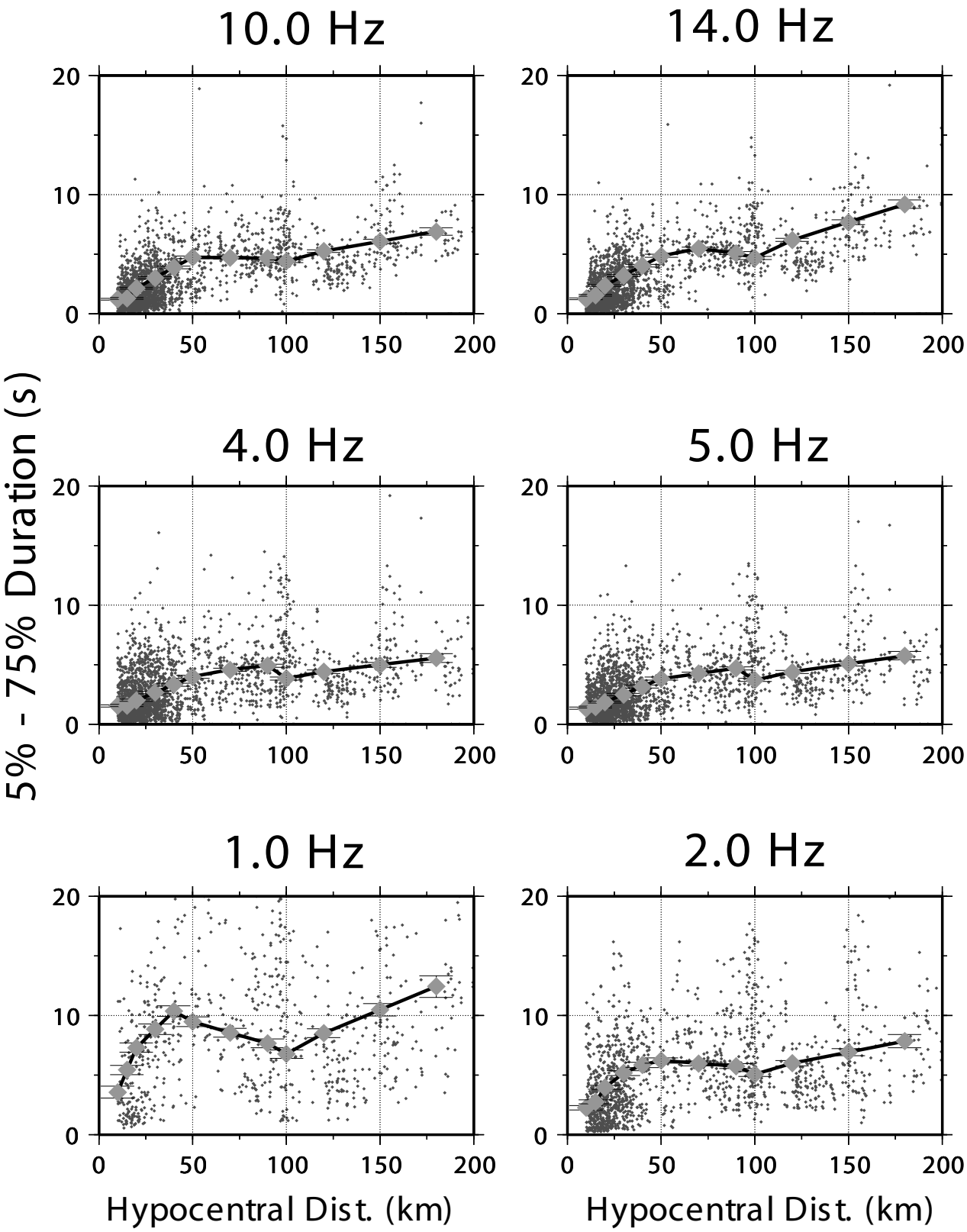
10.0 Hz
14.0 Hz
4.0 Hz
5.0 Hz
1.0 Hz
2.0 Hz
5% - 75% Duration (s)
Hypocentral Dist. (km)
Hypocentral Dist. (km)
0
10
20
0
50
100
150
200

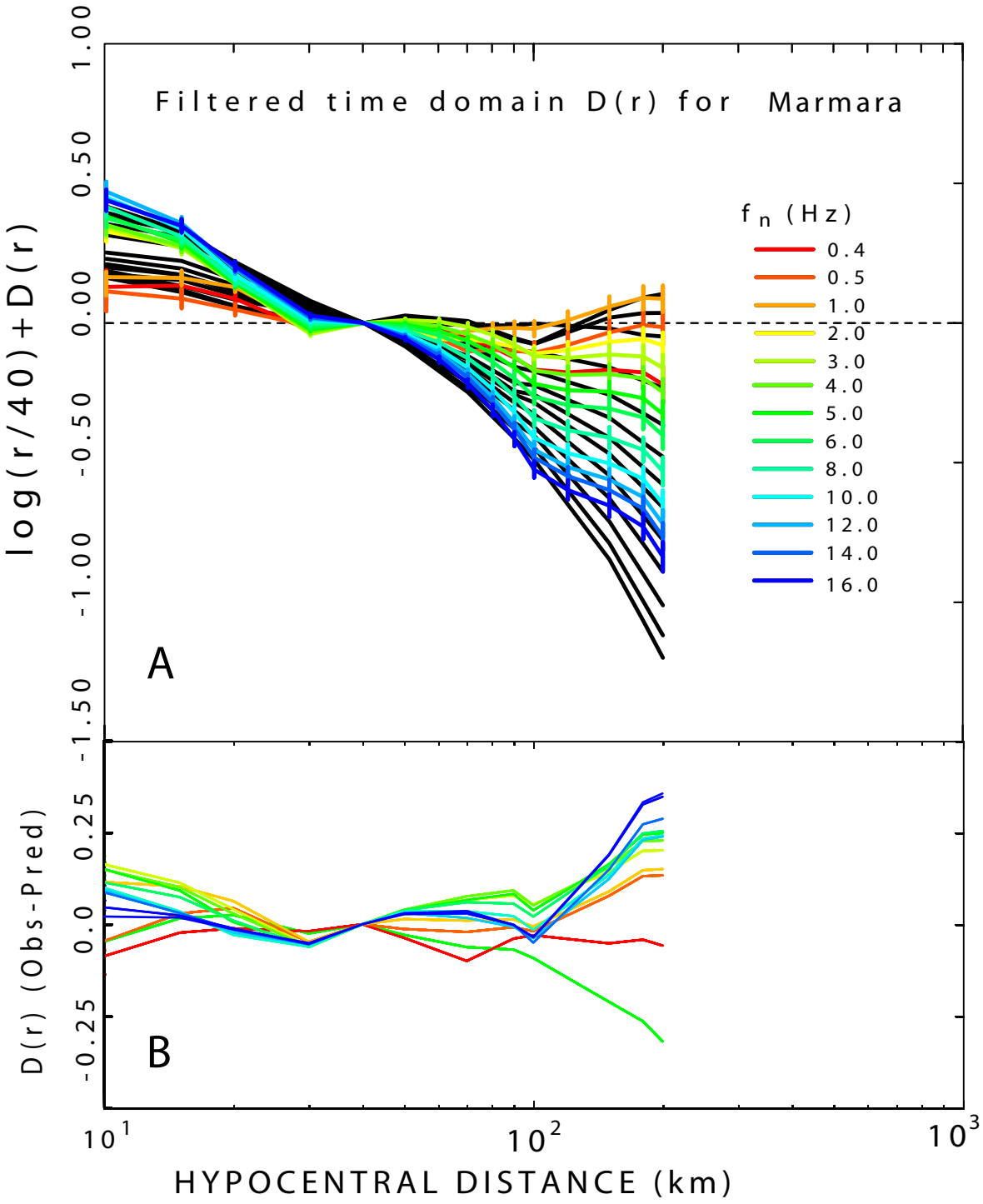
Filtered time domain D(r) for Marmara
log(r/40)+D(r)
1.00
0.50
0.00
-0.50
-1.00
-1.50
A
f n (Hz)
0.4
0.5
1.0
2.0
3.0
4.0
5.0
6.0
8.0
10.0
12.0
14.0
16.0
D(r) (Obs-Pred)
0.25
0.0
-0.25
B
10 1
10 2
10 3
HYPOCENTRAL DISTANCE (km)

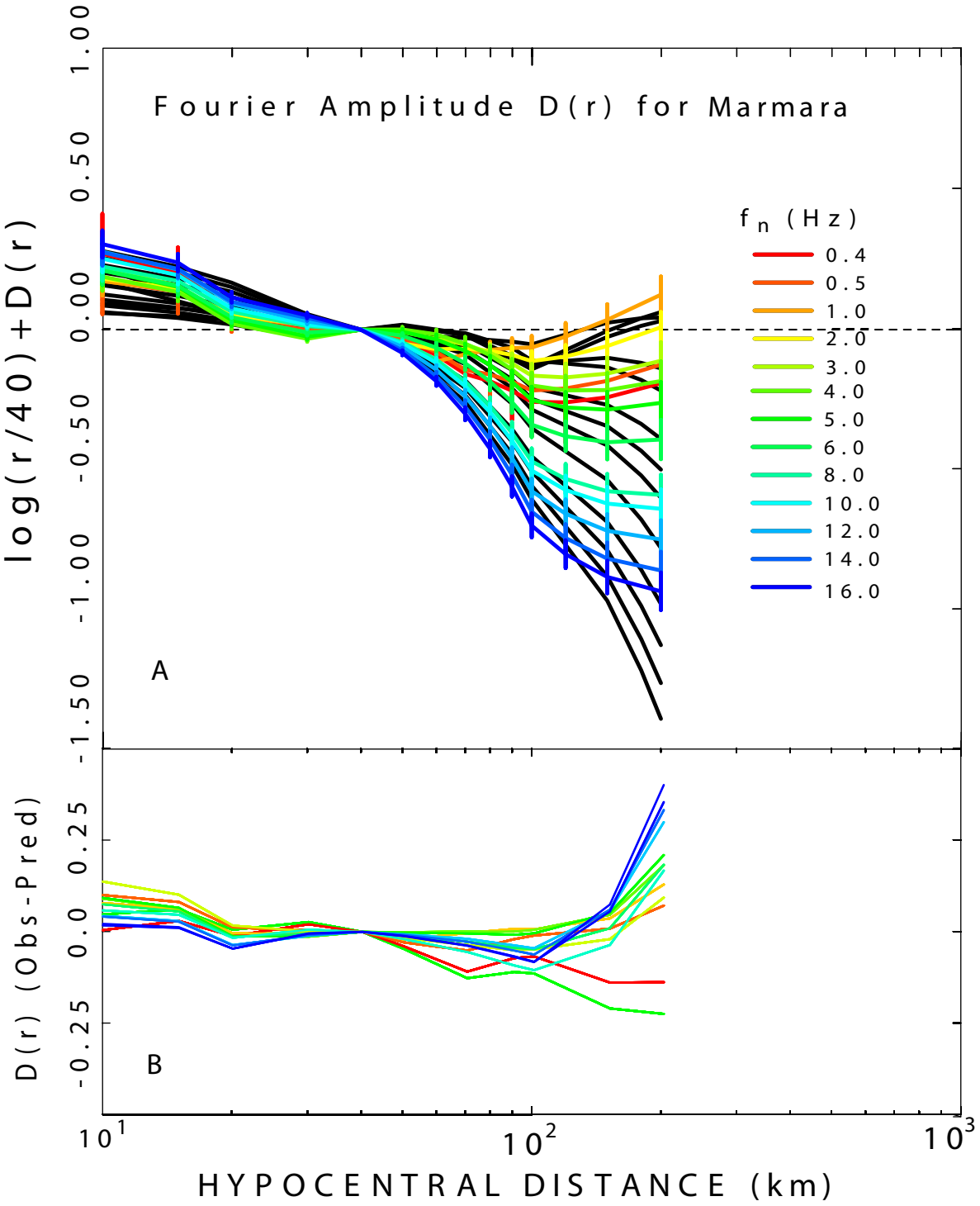
Fourier Amplitude D(r) for Marmara
log(r/40)+D(r)
1.00
0.50
0.00
-0.50
-1.00
-1.50
A
B
D(r) (Obs-Pred)
0.25
0.0
-0.25
f_n (Hz)
0.4
0.5
1.0
2.0
3.0
4.0
5.0
6.0
8.0
10.0
12.0
14.0
16.0
10^1
10^2
10^3
HYPOCENTRAL DISTANCE (km)

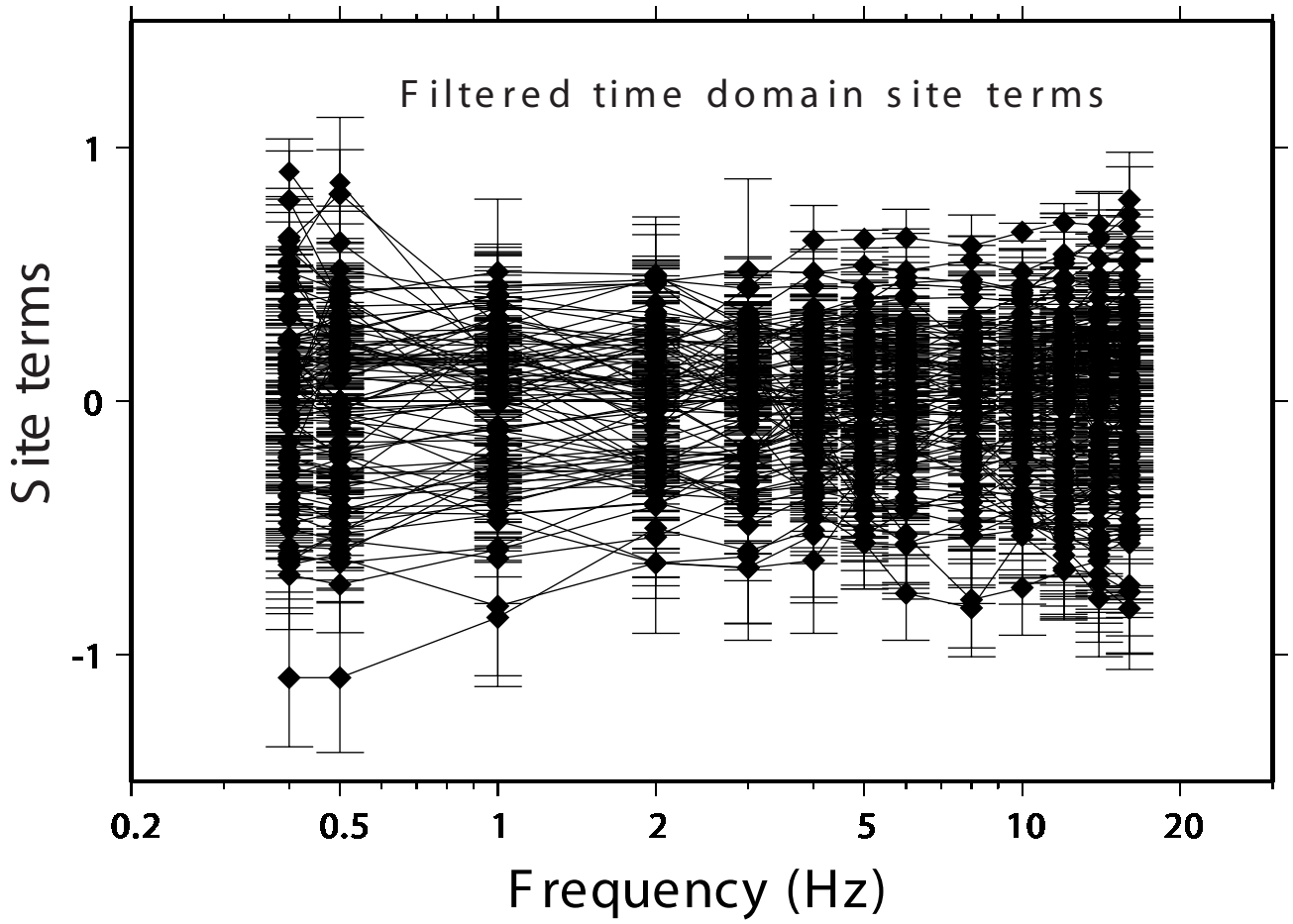
Filtered time domain site terms
Site terms
1
0
-1
0.2
0.5
1
2
5
10
20
Frequency (Hz)

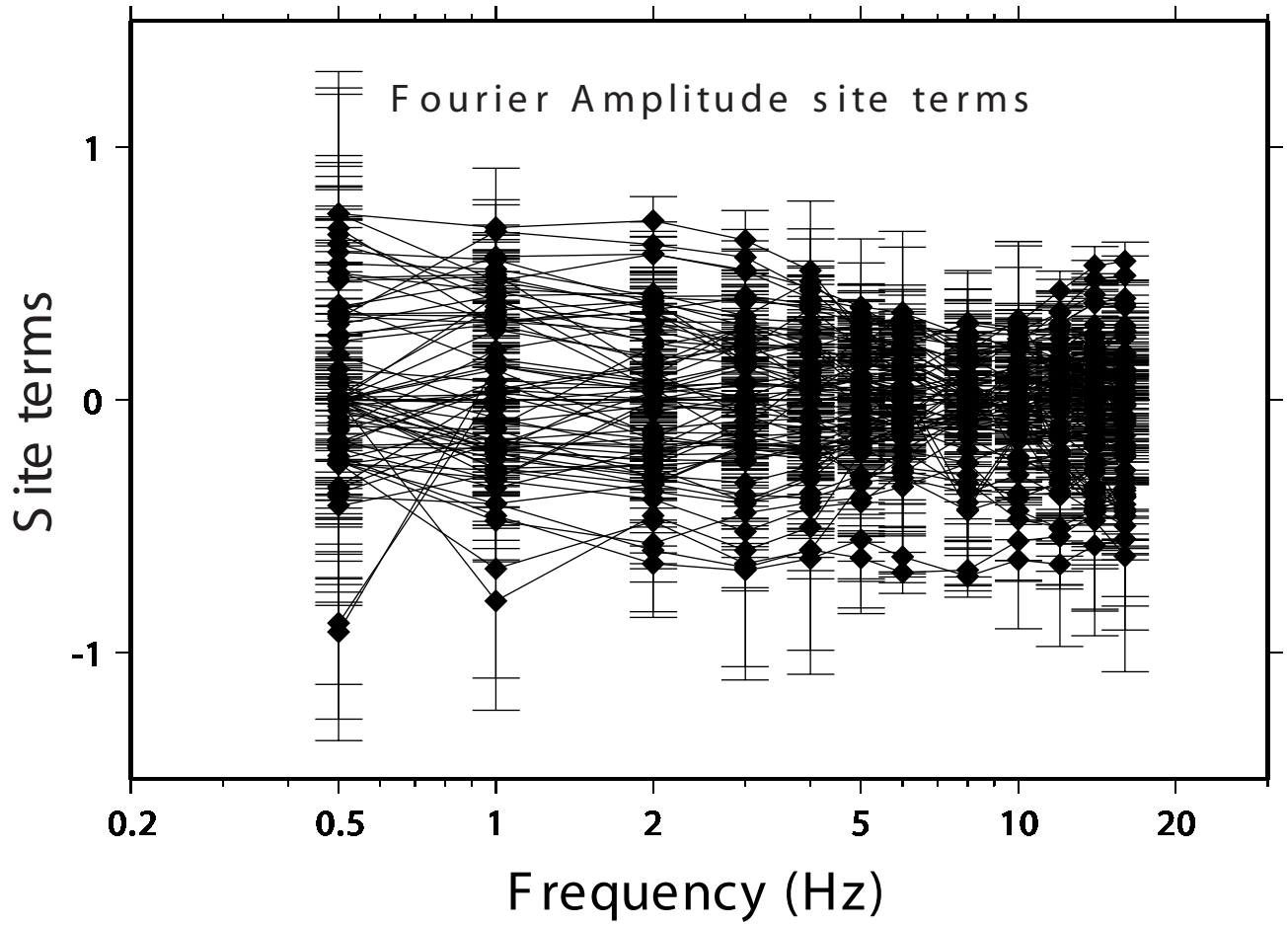
Fourier Amplitude site terms
Site terms
1
0
-1
0.2
0.5
1
2
5
10
20
Frequency (Hz)

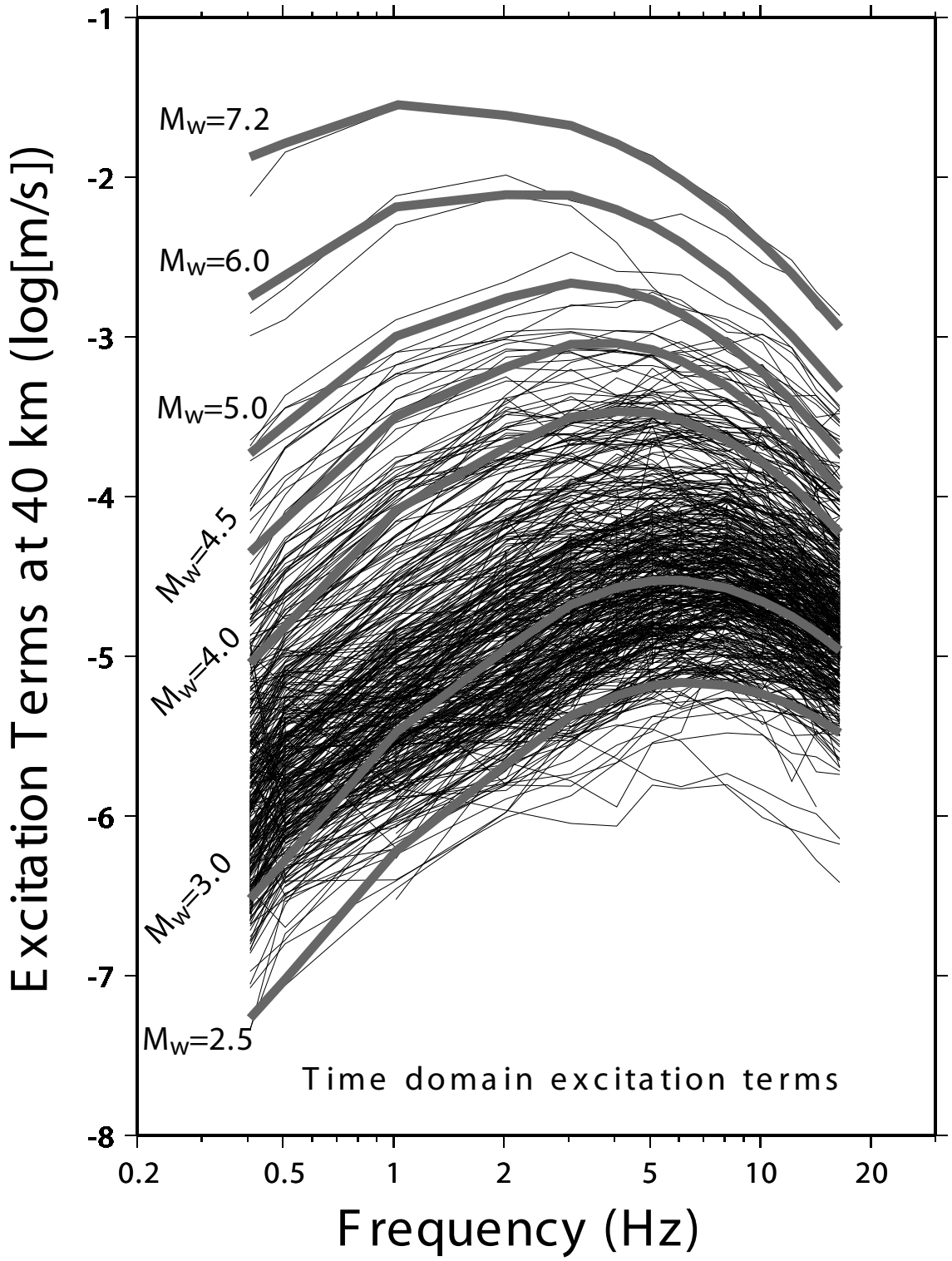
Excitation Terms at 40 km (log[m/s])
Frequency (Hz)
-1
-2
-3
-4
-5
-6
-7
-8
0.2
0.5
1
2
5
10
20
Mw=7.2
Mw=6.0
Mw=5.0
Mw=4.5
Mw=4.0
Mw=3.0
Mw=2.5
Time domain excitation terms

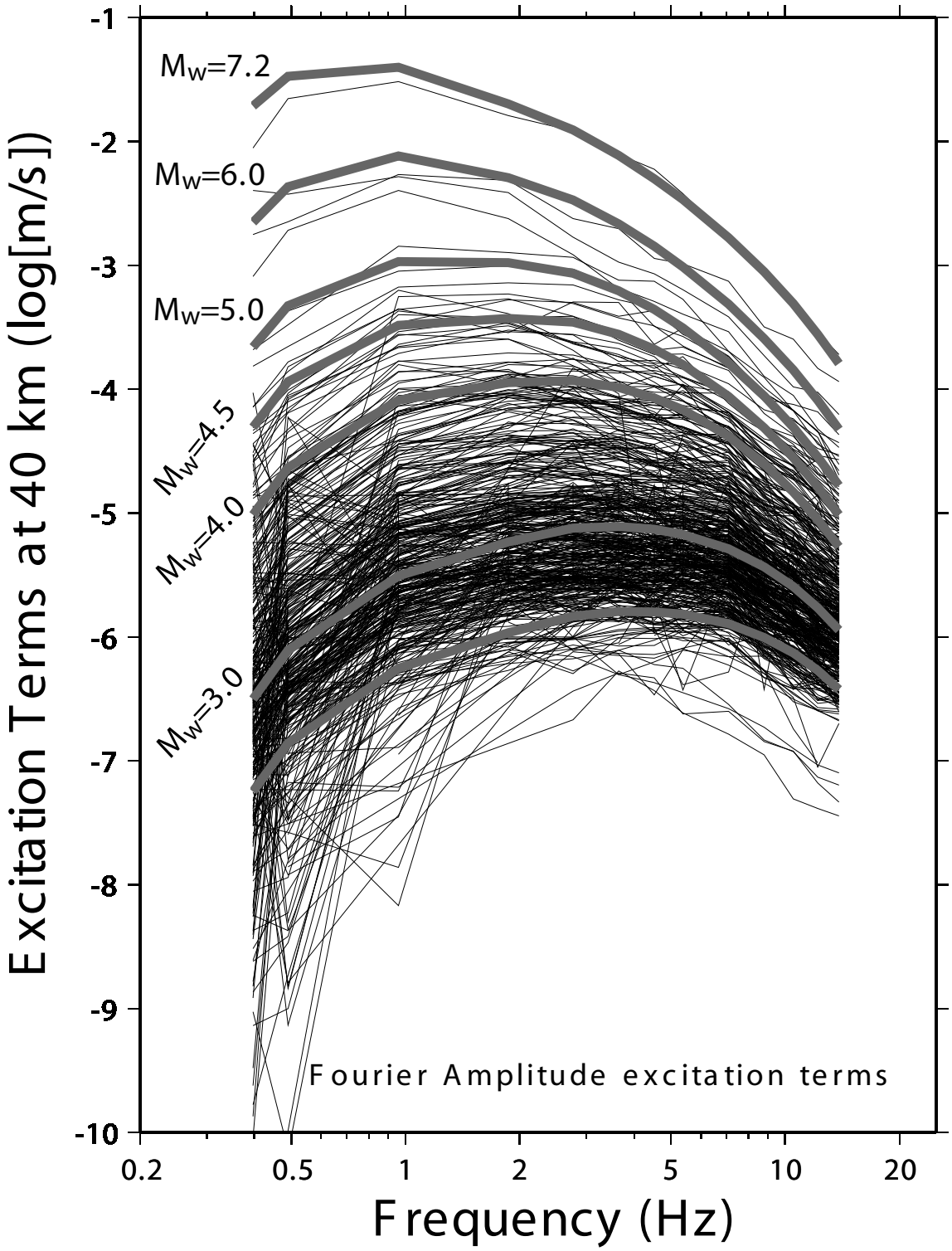
Excitation Terms at 40 km (log[m/s])
Frequency (Hz)
Mw=7.2
Mw=6.0
Mw=5.0
Mw=4.5
Mw=4.0
Mw=3.0
Fourier Amplitude excitation terms
-1
-2
-3
-4
-5
-6
-7
-8
-9
-10
0.2
0.5
1
2
5
10
20

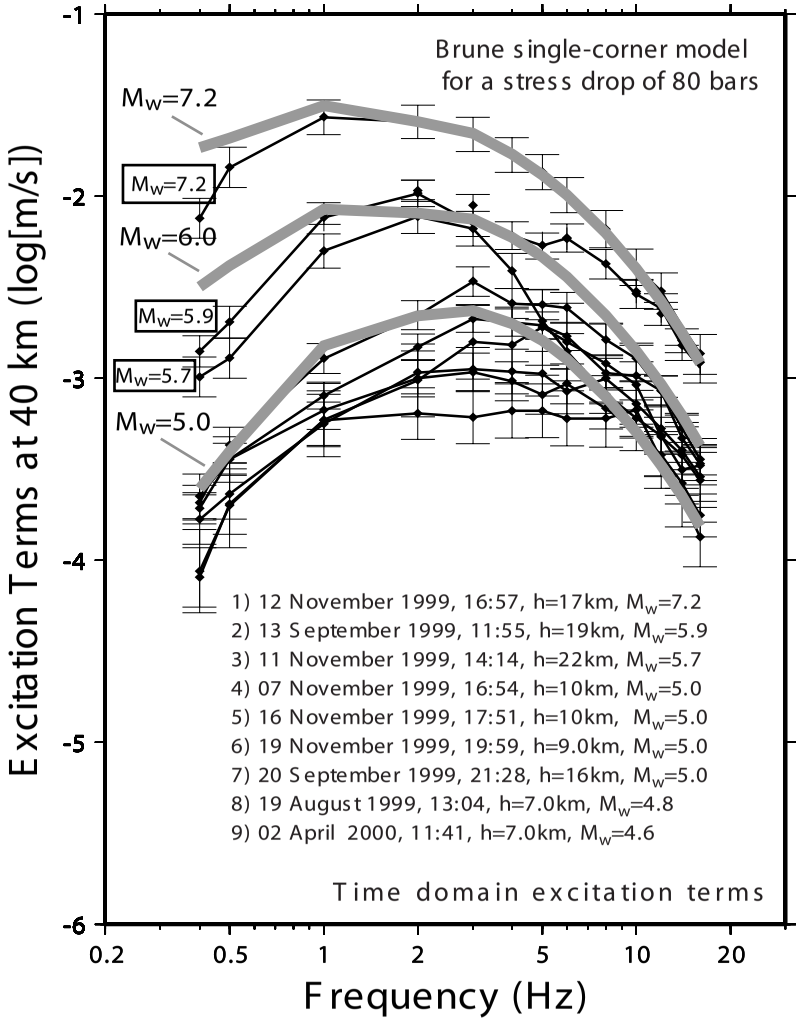
Brune single-corner model
for a stress drop of 80 bars
Mw=7.2
Mw=7.2
Mw=6.0
Mw=5.9
Mw=5.7
Mw=5.0
1) 12 November 1999, 16:57, h=17km, Mw=7.2
2) 13 September 1999, 11:55, h=19km, Mw=5.9
3) 11 November 1999, 14:14, h=22km, Mw=5.7
4) 07 November 1999, 16:54, h=10km, Mw=5.0
5) 16 November 1999, 17:51, h=10km, Mw=5.0
6) 19 November 1999, 19:59, h=9.0km, Mw=5.0
7) 20 September 1999, 21:28, h=16km, Mw=5.0
8) 19 August 1999, 13:04, h=7.0km, Mw=4.8
9) 02 April 2000, 11:41, h=7.0km, Mw=4.6
Time domain excitation terms
Excitation Terms at 40 km (log[m/s])
Frequency (Hz)
-1
-2
-3
-4
-5
-6
0.2
0.5
1
2
5
10
20

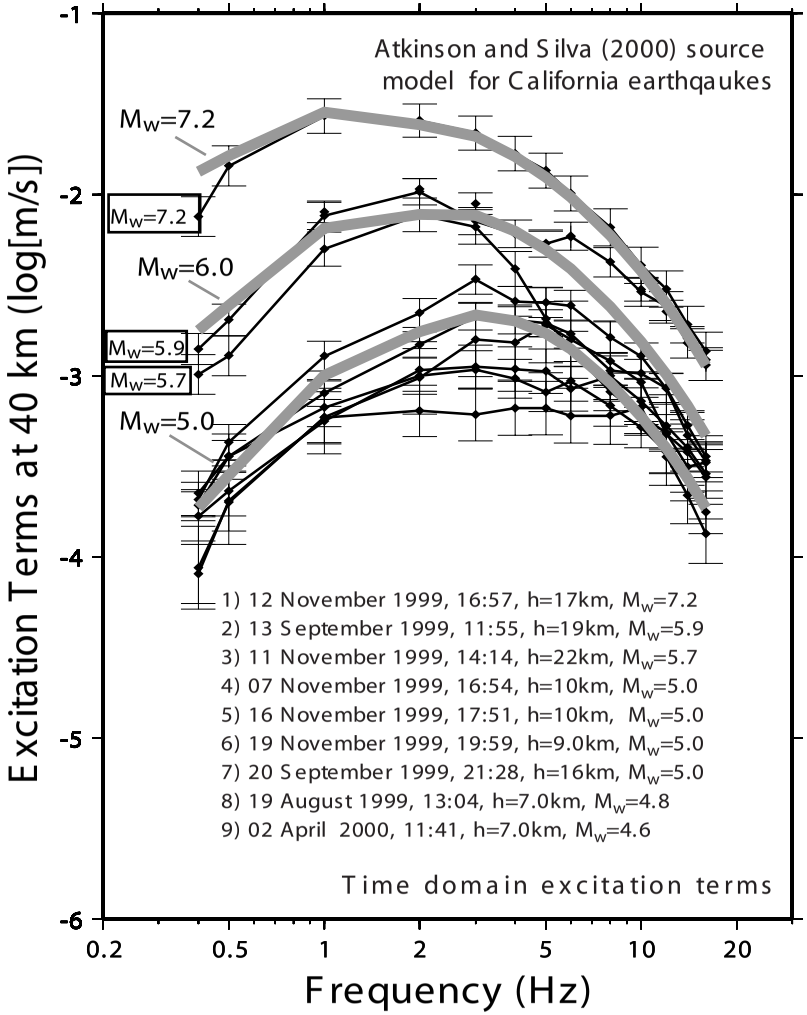
Atkinson and Silva (2000) source
model for California earthqaukes
Mw=7.2
Mw=7.2
Mw=6.0
Mw=5.9
Mw=5.7
Mw=5.0
1) 12 November 1999, 16:57, h=17km, Mw=7.2
2) 13 September 1999, 11:55, h=19km, Mw=5.9
3) 11 November 1999, 14:14, h=22km, Mw=5.7
4) 07 November 1999, 16:54, h=10km, Mw=5.0
5) 16 November 1999, 17:51, h=10km, Mw=5.0
6) 19 November 1999, 19:59, h=9.0km, Mw=5.0
7) 20 September 1999, 21:28, h=16km, Mw=5.0
8) 19 August 1999, 13:04, h=7.0km, Mw=4.8
9) 02 April 2000, 11:41, h=7.0km, Mw=4.6
Time domain excitation terms
Excitation Terms at 40 km (log[m/s])
Frequency (Hz)
-1
-2
-3
-4
-5
-6
0.2
0.5
1
2
5
10
20

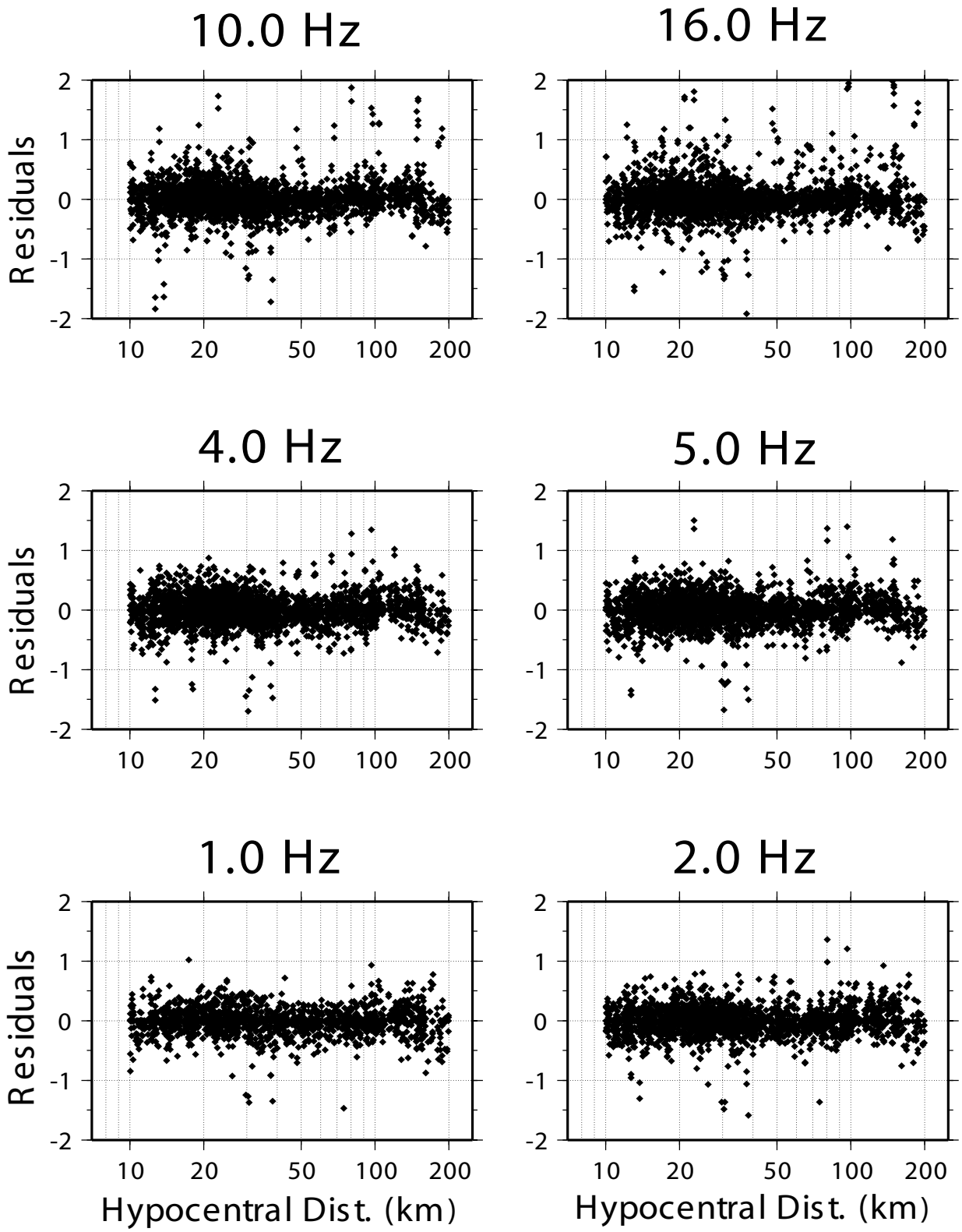
10.0 Hz
16.0 Hz
4.0 Hz
5.0 Hz
1.0 Hz
2.0 Hz
Residuals
Hypocentral Dist. (km)
2
1
0
-1
-2
10
20
50
100
200

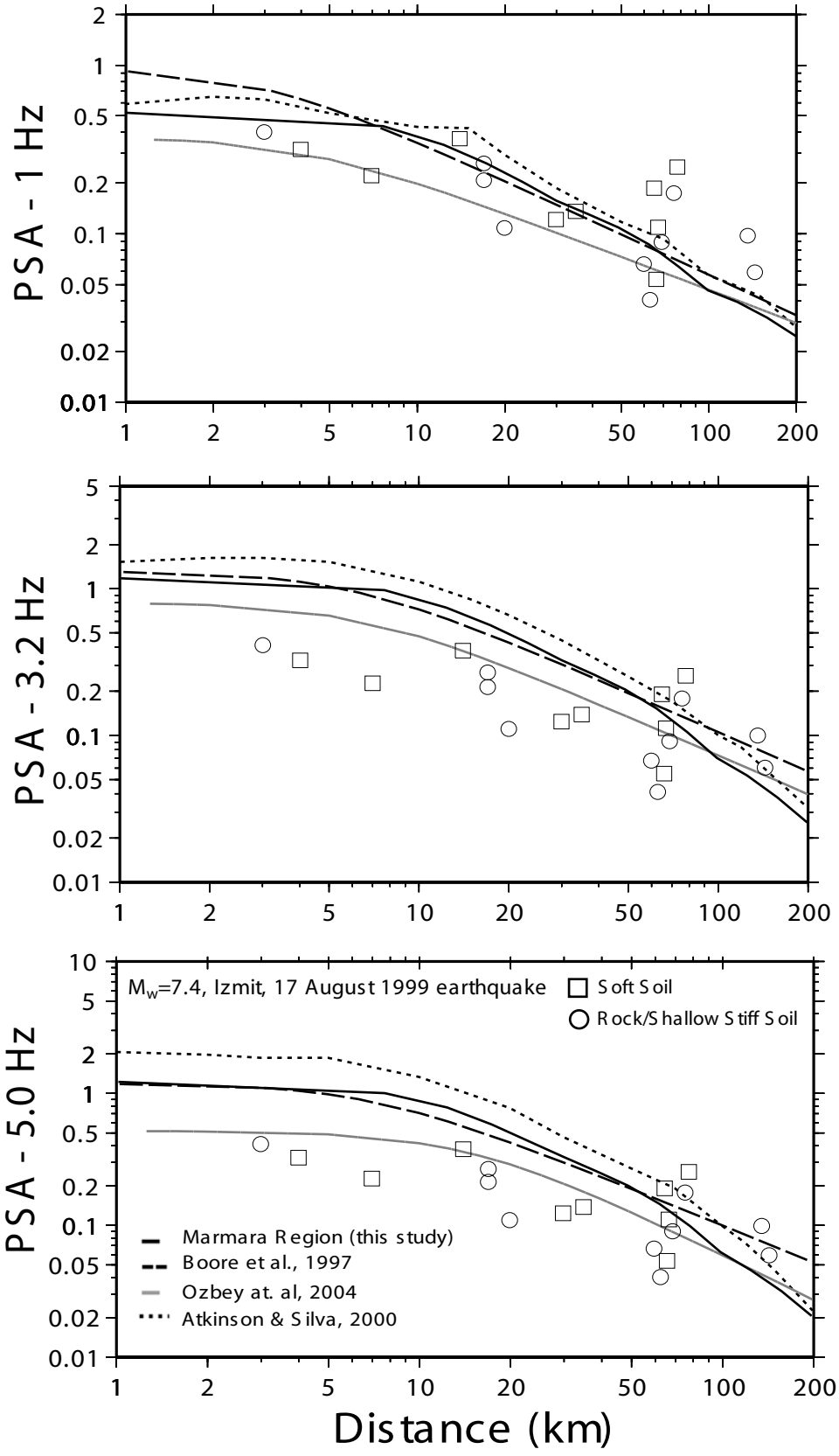
PSA - 1 Hz
PSA - 3.2 Hz
PSA - 5.0 Hz
Distance (km)
M$_w$=7.4, Izmit, 17 August 1999 earthquake
Soft Soil
Rock/Shallow Stiff Soil
Marmara Region (this study)
Boore et al., 1997
Ozbey at. al, 2004
Atkinson & Silva, 2000